water

MDPI

Article

MIS 5.5 Highstand and Future Sea Level Flooding at 2100 and 2300 in Tectonically Stable Areas of Central Mediterranean Sea: Sardinia and the Pontina Plain (Southern Latium), Italy

Giacomo Deiana [1,2,*], Fabrizio Antonioli [3], Lorenzo Moretti [4], Paolo Emanuele Orrù [1,2], Giovanni Randazzo [5] and Valeria Lo Presti [5]

1 Department of Chemical and Geological Sciences, University of Cagliari, 09042 Cagliari, Italy; orrup@unica.it
2 CoNISMa Interuniversity Consortium on Marine Sciences, 00126 Roma, Italy
3 Istituto Nazionale di Geofisica e Vulcanologia (INGV), via di Vigna Murata, 00144 Rome, Italy; fabrizioantonioli2@gmail.com
4 Ente Per Le Nuove Tecnologie, l'Energia e l'Ambiente (ENEA), 40129 Bologna, Italy; lorenzo.moretti@enea.it
5 Department of Mathematics, Physics and Geosciences, MIFT, University of Messina, 98166 Messina, Italy; grandazzo@unime.it (G.R.); valeria.lopresti@gmail.com (V.L.P.)
* Correspondence: giacomo.deiana@unica.it

Abstract: Areas of the Mediterranean Sea are dynamic habitats in which human activities have been conducted for centuries and which feature micro-tidal environments with about 0.40 m of range. For this reason, human settlements are still concentrated along a narrow coastline strip, where any change in the sea level and coastal dynamics may impact anthropic activities. We analyzed light detection and ranging (LiDAR) and Copernicus Earth observation data. The aim of this research is to provide estimates and detailed maps (in three coastal plain of Sardinia (Italy) and in the Pontina Plain (southern Latium, Italy) of: (i) the past marine transgression occurred during MIS 5.5 highstand 119 kyrss BP; (ii) the coastline regression occurred during the last glacial maximum MIS 2 (21.5 krs cal BP); and (iii) the potential marine submersion for 2100 and 2300. The objective of this multidisciplinary study is to provide maps of sea level rise future scenarios using the IPCC RCP 8.5 2019 projections and glacio-hydro-isostatic movements for the above selected coastal zones (considered tectonically stable), which are the locations of touristic resorts, railways and heritage sites. We estimated a potential loss of land for the above areas of between about 146 km^2 (IPCC 2019-RCP8.5 scenario) and 637 km^2 along a coastline length of about 268 km.

Keywords: central Mediterranean coastal plains; past (MIS 5.5) and future sea level at 2100 and 2300; Sardinia; Pontina Plain

Citation: Deiana, G.; Antonioli, F.; Moretti, L.; Orrù, P.E.; Randazzo, G.; Lo Presti, V. MIS 5.5 Highstand and Future Sea Level Flooding at 2100 and 2300 in Tectonically Stable Areas of Central Mediterranean Sea: Sardinia and the Pontina Plain (Southern Latium), Italy. *Water* **2021**, *13*, 2597. https://doi.org/10.3390/w13182597

Academic Editor: Monica Papini

Received: 2 August 2021
Accepted: 14 September 2021
Published: 21 September 2021

1. Introduction

Sea level rise is one of the most important consequences of climate change [1] which strongly affects global communities and human settlements along the coast. The main responsible factors are global warming, which is driving the melting of ice and the thermal expansion of the oceans [1] and finally the geological vertical movements of the land along the coastal zones, which may accelerate (or decrease) the submersion of low-elevated coasts [2–5]. In this scenario, the coastal lowlands will be more prone to marine flooding during extreme sea events, threatening many highly populated areas of the Mediterranean coasts [3,4].

Future warming on the Mediterranean Sea could provide a higher sea level rise than published in the 2019 IPCC report [1]. Much research was recently published on the effects of sea level rise on the Mediterranean coasts [2–5]. For much of the Italian coast, adding local factors (tectonic and isostasy) to the global climate signal projections for future sea level rise results in an increasing vulnerability of the littoral zones and coastal plains. In the above studies, in order to provide the relative sea level rise projections for the

preparation of flooding scenarios maps at 2100, the authors applied a multidisciplinary approach that includes sea level rise estimates as obtained by the IPCC (www.ipcc.ch—accessed on 20 June 2021), Rahmstorf 2007, detailed geomorphological information and land topography; coastal inundation projection maps were produced through the use of available high-resolution lidar data.

In this research we use the methodologies tested in previous works [2] where the relative sea level is the sum of eustasy, isostasy and tectonic movement. We used the IPCC 2019 AR 8.5 projections for the sea level rise expected at 2100 [6]. The objective of our work is to highlight at what altitude can the fossil signs of maximum marine ingression (forms and aged deposits) now be observed, which occurred during MIS 5.5 compared with the sea level projections for 2100 and 2300 (IPCC 2019) in the four coastal sites under study (Figure 1). We also take in consideration the MIS 5.5 maximum highstand comparing the observed data in field with the ice model [7] projections for Sardinia and the Pontina Plain. In addition, on the basis of the bathymetry and the available data and models, we positioned the 21.5 ka cal BP coastline reached during the LGM (last glacial maximum) on the continental shelf in front of the Plains. Furthermore, on the basis of the IPCC projections we have calculated (adding the geological vertical movements) the altitude at which the sea will be reached (according to the AR 8.5 scenario) at 2100 and 2300. We have chosen these sites because they are located in Sardinia, one of the most stable areas of the Mediterranean and in Southern Lazio, a similar stable coastal area [8] but with high rates of subsidence partly due to tectonics and partly due to the drying of the peat drained by the reclamation of the 1930s and 1940s.

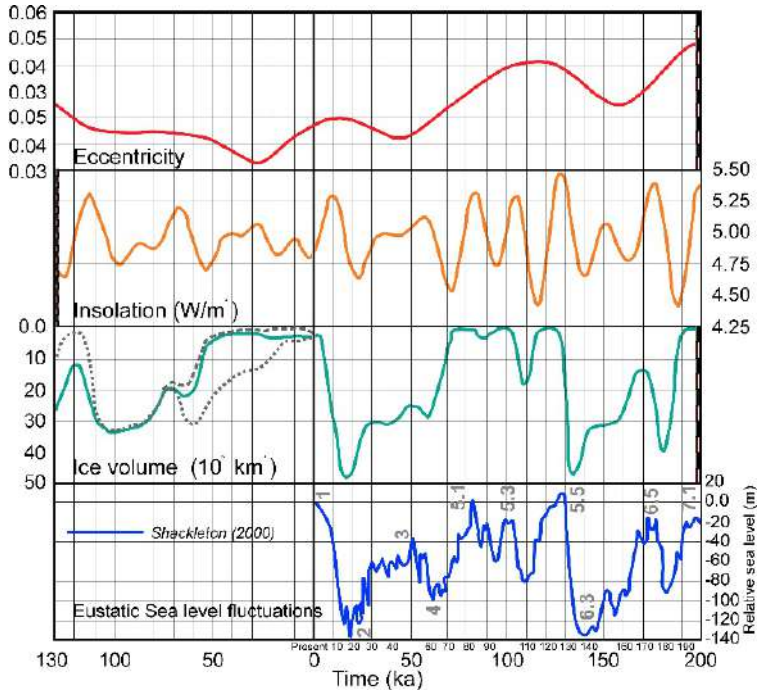

Figure 1. Long-term variations of eccentricity (**top**), June insolation at 65° N (**middle**), and simulated Northern Hemisphere ice volume (increasing downward) (**bottom**) for 200,000 years before the present to 130,000 from now. Time is negative in the past and positive in the future. In the Ice volume graphic for the future, three CO2 scenarios were used: last glacial–interglacial values (green solid line), a human-induced concentration of 750 ppmv (grey dashed line), and a constant concentration of 210 ppmv (grey dotted line). In the Eustatic Sea level fluctuation graphic the gray numbers represent the Medium isotope stages. Simulation results from [9,10]; eccentricity and insolation from [11]. Figure modified from [10,12].

2. Materials and Methods

An innovative methodology made for the first time for drafting the sea flooding maps, was to "look" not only to the future (2100, 2300) but also to the past. We indagated in the studied areas in order to understand what the effects of the maximum transgression of the last highstand were (MIS 5.5 that occurred between 126 and 119 ka BP); this choice is due to very specific reasons. There is a generalized belief that since the maximum insolation on Earth ceased about 6000 years ago (climatic optimum) we are "walking" towards an ice age. The durations of the last warm periods (MIS 5.5, MIS 9, MIS 11, etc.), have always been around 10–11 thousand years [13]. However, if it is true that at 119 ka BP there was a maximum of insolation of about 550 W/m^2, calculated for 65° in June, it is also true that during the climatic optimum (about 6, ka BP) l insolation was of a lesser entity: 520 W\m^2. Subsequently: (1) the insolation has been decreasing, and (2) the climate does not seem to have cooled. In a quoted article [14], entitled "An exceptional long Interglacial period?", the authors show that due to a particular movement of eccentricity the "warm-hot" climatic period, instead of taking us towards an ice age (as happened in the last 4 highstand on earth), should last at least another 50 ka (Figure 1): "But more recent studies point toward a different future: a long interglacial that may last another 50,000 years".

At 119 ka BP, the insolation was higher than today, the sea was about 8 m higher [7], but the CO_2 content in the atmosphere never exceeded 295 ppm. Meanwhile, today, with a lower insolation, but a much higher content of CO_2, 415 ppm, we can also observe a sea level 8 m lower than 119 ka BP and a rise that exceeds the acceleration of 3 mm/year. The IPCC 2019 projections estimate (using the RCP 8.5 scenario) a rise higher than one meter for the next 79 years (2100). The CO_2 increase would also further delay the triggering of a cold period.

This research is based on the method described in [3], and [15], to ensure homogeneity and enable a comparison with previous results, extending the study toward other central Mediterranean coastal plains, besides Italy. The sea level change along the Mediterranean coast is the sum of eustatic, glacio-hydro-isostatic and tectonic factors. The first is time dependent while the latter two also vary with location, and they consist to sum the different components of sea level rise in the following main steps: (a) the IPCC AR5 projections (RCP-8.5 upper limits scenarios reported in the IPCC 2019); (b) the long-term land vertical movements from geological data [7,8,16]; (c) the glacio-hydro-isostatic movement (GIA) [2]; (d) by combining eustatic, isostatic and tectonic data projected up to 2100, and 2300, we provided the expected sea levels at 2100 and 2300 for the investigated coastal areas and the expected inland extent of related marine flooding.

We underline our choice to use the global IPCC AR5 data for the projections to 2100, even if some works have been published for the Mediterranean that take into account SST, evapotranspiration and salinity [17] and publish projections a few decimeters lower than the global data we used. However, SSTs in the Mediterranean show very different values across the whole basin and the available data [17] relate to the entire Mediterranean. We therefore decided to use IPCC AR5 which contains a literature of thousands of publications. After submitting the manuscript, the IPCC AR6 report was published where regional projections are also taken into consideration. In particular, for the Mediterranean there is the Cagliari data which are 0.78 $\pm$ 0.3 m [18]. This number (also considering the error) is quite similar to that expected for Cagliari (Table 1: IPCC 2100 median range 0.89).

The choice of the study areas was decided by several different factors: (i) tectonics (stable areas only); (ii) exposure; (iii) max fetch; (iv) sedimentological material; (v) wave energy flux; (vi) bedrock; and (vii) geomorphological features. Our maps show the maximum sea level height expected for 2100 and 2300 for the above referenced climatic projections and the corresponding flooded area. Sea level rose rapidly between 21 and about 4 ka years ago. Over the last 100 years the sea level has risen globally by 18 cm, and by 14 cm (on average 1.4 mm /year) in the Mediterranean Sea. The little differences between the global and a lower rise of the Mediterranean, considered a closed basin, are due to evapotranspiration and to an increasingly limited flow of rivers.

We remark that our analysis does not take into account hydrodynamics models, and the contribution of sediment flow from rivers, coastal erosion and all the possible anthropic defences that may change the estimated extension of the flooded areas proposed in this study.

Table 1. a: site; b: (digital terrain model, DTM) resolution and accuracy; c: epoch of DTM; d–g: IPCC projection AR5-RCP8; h: glacial isostatic adjustment (GIA) rate [2]; i: vertical tectonic rate mm/year; l–o: relative sea level rise for 2100, 2300, IPCC AR5-RCP 8.5 scenarios.

N	a Site	b DTM Resolution ± Vertical Accuracy (m)		c Map Year	d Projection 2100 IPCC 2019 AR 8.5, Upper Likely Range mm	E Projection 2100 IPCC 2019 AR 8.5, Median Range mm	F Projection 2300 IPCC 2019 AR 8.5, Upper Likely Range mm	g Projection 2300 IPCC 2019 AR 8.5, Median Range mm	h GIA mm/y	i Vertical Movements mm/y	l Total mm IPCC 2100 Upper Likely Range	m Total mm IPCC 2100 Median Range	n Total mm IPCC 2300 Upper Likely Range	o Total mm IPCC 2300 Median Range
1	Cagliari	LIDAR 5×5 (± 0.2)	EMODNET 85×85 (± 1.0)	2008	1100	840	5200	3700	0.57	-	1152	893	5252	3752
2	Oristano	LIDAR 1×1 (± 0.2)	EMODNET 85×85 (± 1.0)	2008	1100	840	5200	3700	0.57	-	1152	893	5252	3752
3	Olbia	LIDAR 1×1 (± 0.2)	EMODNET 85×85 (± 1.0)	2008	1100	840	5200	3700	0.62	-	1157	897	5256	3756
4	Pontina	25×25 ± 1	EMODNET 85×85 (± 1.0)	2010	1100	840	5200	3700	0.44	−0.1	1149	889	5249	3749

2.1. Field Work

2.1.1. Pontina Plain

For the Pontina Plain, some papers published in the 1930s and 1950s were carefully considered, and the altitude of the fossil deposit containing *Persistrombus latus* or Senegalese fauna was also revised in field (with respect to reviews [8] and [19]), lowering it from +10 to +5.3 m. In addition, some new lagoonal fossil layers containing Cerastoderma edulis have been found in the field. These lagoonal levels outcropping in the eastern portion of the Pontina Plain, between +4 and −2 m, were outcrops only if incised by the 1930s' "Bonifica" channels whose cleaning revealed the fossil levels. We checked what was published in [20], in 3 outcrops on the field. The altitudes were re-measured on Google Earth maps (which presents a very precise altimetry in the flat areas: see also Materials and Methods [15]).

2.1.2. Sardinia

As part of this work, the stratigraphic and chronological point of view of deposits containing *Persististrombus latus*, *Patella ferruginea*, etc., have been reviewed, and detected in previous studies [21–23] at altitudes between +4.0 m and +8.0 m a.s.l. The levels containing lagoon fossils with *Cerastoderma edulis* were found in the plains of Cagliari (Elmas-Assemini plane) and of Oristano (north of the Cabras lagoon). The respective elevations were determined through measurements with a DGPS antennas: Trimble R8s model. The planimetric and altimetric surveys were carried out operating in static mode. The raw DGPS data have been processed using the Trimble Business Center software (V. 2.50). The processed data have an accuracy of $\pm 1 \div 2$ cm.

2.2. Digital Terrain Models

To map the sea level rise scenarios, a data set of high-resolution topography based on light detection and ranging (LiDAR) observations produced by different agencies from 2008 to 2019 was used (Table 1). The extracted digital terrain models (DTM) were obtained at variable spatial resolutions depending on the data set and in the range at about 20 cm of mean vertical resolution [24]. The details of the characteristics of the DTM are described in Table 1 and in the maps available in the online supporting material.

To link the land surface to the seafloor along the coasts and represent MIS 2 sea level, the bathymetric data were obtained from the European Marine Observation and Data Net-

work (EMODnet, http://portal.emodnet-bathymetry.eu/ [25]—(accessed on 16 December 2020). The DTM has been generated from selected bathymetric survey data sets, composed by DTMs and satellite derive bathymetry (SDB) data products, while gaps of no data coverage were completed by integrating the GEBCO digital bathymetry. The spatial resolution of this DTM was 85 × 85 m while the vertical resolution was 1 m. However, the use of different resolution DTMs for the emerged and submerged part did not lead to differences in the elaboration of flood models; this is mainly due to the fact that the high-resolution DTM was available for the entire emerged sector, up to the current coastline.

Marine and terrestrial topographic data were co-registered and georeferenced into the same UTM-WGS84 (Zones 32 and 33) reference frame, and the shoreline position was determined relative to the epoch of the surveys for each area. The details regarding the link to the website from which we downloaded or requested the digital data are also described in the online supporting material.

The DTMs were mapped and analyzed by Global Mapper Software® (www.globalmapper.com [26]—accessed on 10 June 2020) (Version 21, Hallowell, ME, USA) to create 3D high-resolution maps of the investigated areas, on which the position of the present-day coastline and its potential position in 2100 as a result of relative sea level rise are shown by contour lines. The DTMs with contour lines and submerged surfaces were represented using the color-shaded option and exported as georeferenced images through the GIS composer (Tables 1 and 2).

Table 2. Modelled and observed altitude during LGM (21.5 kyrs cal BP) and MIS 5.5 (119 Kyrs BP).

Sites	Altitude LGM Model, [2]. m	Altitude LGM Model, [27]. m	Observed LGM Altitude. m	Altitude MIS 5.5 Model, [7]. m	Observed MIS 5.5 Altitude. m This Paper
Cagliari	−129.2	−122	−125	+8.4	+4.8
Oristano	−126.8	−124	−130	+8.6	+6.5
Olbia	−127.5	−122	−126	+8.5	+4.9
Pontina	−117,8	−117	——	+8.2	+7.96, −12

3. Results

3.1. Geomorphology and Altitude of MIS 5.5 in Sardinia Sites

3.1.1. Cagliari Coastal Plains

The coastal sector of Campidano graben of Cagliari (Figure 2), is articulated in two coastal plains with different geodynamic evolutions: the eastern plain is set on a graben structure active until the upper Miocene, while the western plain is set on a graben active until the lower-middle Pleistocene.

The stratigraphy section of Sant'Elia Cape represents a closure towards the sea of the Cagliari hills horst structure, where A. Lamarmora, in 1856, surveyed for the first time the last interglacial stratigraphic succession. Later, this stratigraphic section was indicated as the locus typicus of the "Tyrrhenian plane" [21], an attribution confirmed by U/Th isotopic dating corals [8,22,23]. The maximum sea ingression altitude of the sea during MIS 5.5 formed two deep bays separated by the Cagliari hills promontory and the paleo island of Sant Elia and Sella del Diavolo reliefs. Afterwards, sedimentation from two tributary rivers (Rio Mannu-Cixerri to the west and Riu Saliu and Cungiaus to the east) led to the emersion of the Sa Illetta barrier islands forming the actual Santa Gilla Lagoon (western sector) and to the formation of the Is Arenas littoral spit closing the Molentargius paleo-lagoon (eastern sector). Evidence of the shoreline of MIS 5.5 maximum ingression was reported by Segre [28], in the Elmas coastal plain, behind the innermost part of the Santa Gilla lagoon, represented by a coastal gravel deposit in a fossiliferous sandy matrix of *Cerastoderma glaucum*.

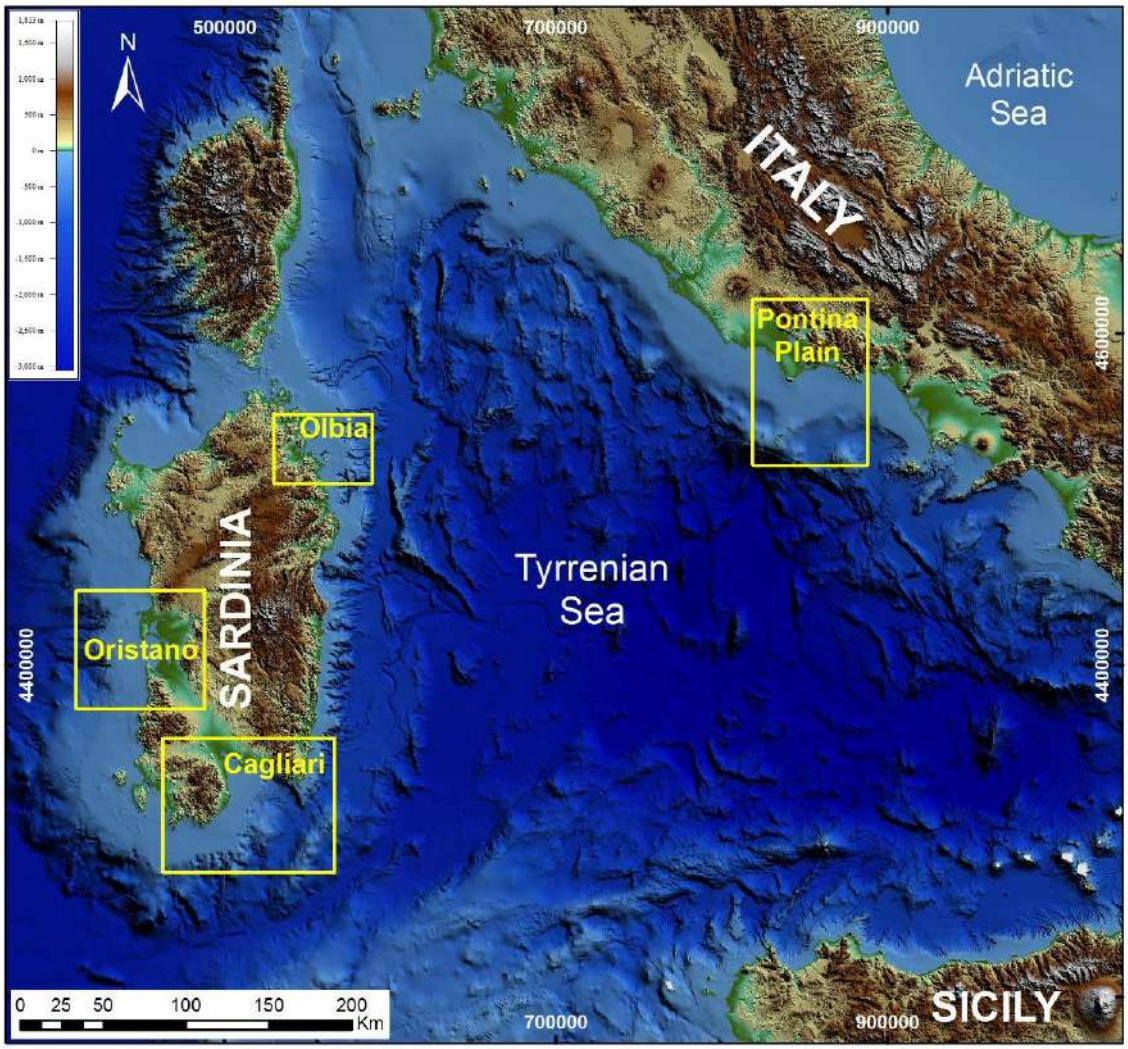

Figure 2. Overview map of the central Mediterranean region showing the locations (red dots) of the coastal plains studied.

During observations for the study of the Holocene sea rise, the site described by Segre [28] and Orrù [29] was detected; in the present work, the inner margin of the MIS 5 transgression was recognized in both Santa Gilla and Molentargius coastal plains, represented by a bank erosion incised in Middle Pleistocene alluvial deposits (MIS 6) on which they rest in onlap.

The MIS 5.5 marine littoral depositional terraces are composed by predominantly quartzose gravels at the elevation of +3.8 m in the western sector (Elmas-Assemini plain), (Figures 3 and 5, Section 5) and of fossiliferous sandstones with inclined lamination at the maximum elevation of 4.80 for the eastern sector (Pirri-Monserrato plain) (Figure 5, Section 4). The lower elevation of the Elmas marine terrace could be related to the greater incidence of the western plain subsidence, as hosted in a structure with recent tectonic activity.

The paleo barrier island of Sa Illetta has a maximum elevation of MIS 5 littoral deposits at +4.30 m in correspondence with a bioconstructed reef with corals (Cladocora coespitosa) and red algal associations of *Litophyllum* [30] (Figure 5, Section 2 and Figure **??**). Comparative U/Th and aminostratigraphic analyses on corals have attributed an age of −149 10 kyrs BP [23]); a similar chronostratigraphic placement based on ESR analyses on Arca noae [30] presented littoral deposits of the Is Arenas paleo-beach that reached a maximum altitude of +4.5 m (Figure 5, Section 3).

During the excavation of the access channel to the container port of Cagliari, a tanatocenosis of Persististrombus latus −10 m was sampled (Figure 5, Section 1). We describe in this paper a new section of the same level at −16.50 m, analysed during a dive survey in the deepening area of the outer channel.

Geophysical surveys (seismic profile, [29]) allowed the following of the paleo-valleys (mostly buried) carved during the MIS 2, these cross the whole platform until they reach the shelf break where they contribute to the construction of low stationing terraces (LGM paleo-sea levels); they are sometimes involved in mass gravitational movements [31].

A Punic paleo-sea level (2500 cal BP) buried at −2 m is preserved in the innermost area of the Santa Gilla lagoon [32–34].

Figure 3. Aerial photograph of the coastal plain of Cagliari showing the main geomorphological features, yellow dashed line indicates the paleo high sea level of MIS 5.5 "Tirreniano"; the littoral deposits of the last interglacial (LI) and the Holocenic shore deposits. Location of MIS5 stratigraphic sections: Section (1), geological profile crosses the container port for 4 km; Section (2), the north face of a large paleo barrier island of the MIS 5.5 of Sa Illetta in front of Santa Gilla lagoon [23]; Section (3), located in a quarry in the littoral paleo spit of Is Arenas; Section (4) and (5), marine terraces at the inner margin of the MIS5.5 transgression overlapping fluvial deposits of MIS 6; Section (6). MIS5 deposits intercepted from the dredging embankment at −16.5 m, 4 m below in the seabed.

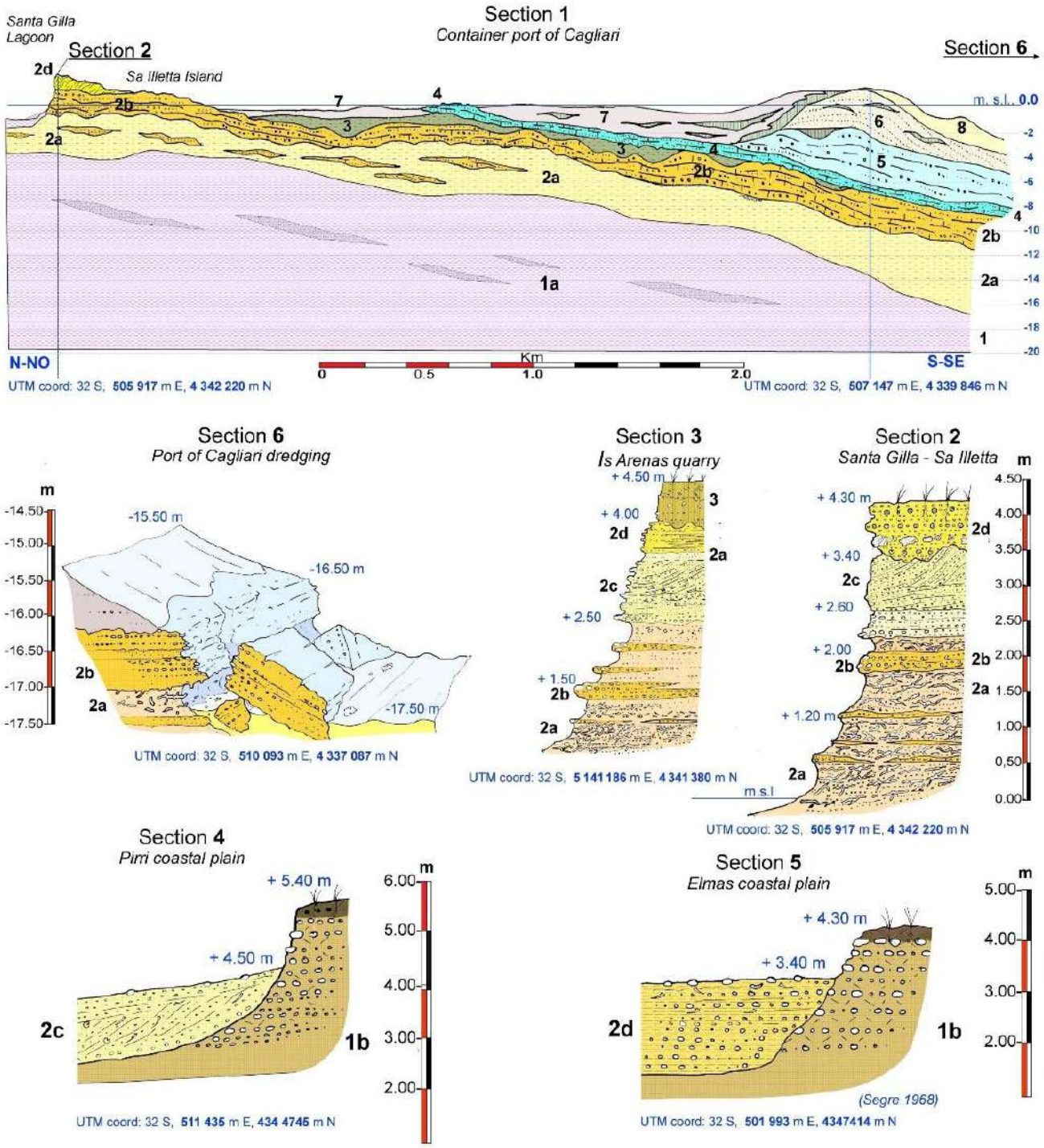

Figure 4. Stratigraphic sections of the MIS 5.5 sequences in the Cagliari coastal plain. (1a) (Section 1): deltaic complex in silt and sandy silt with clay and sand with *Ostrea sp.* in lenses (MIS 6); (1b) (Sections 4/5): fluvial deposit with polygenic and heterometric pebbles in oxidized clayey silt matrix, weakly cemented (MIS 6); (2a): mainly sandy littoral deposit irregularly cemented with burrows bioturbation structures, containing *Persistisstrombus latus* e *Cerastoderma glaucum* (MIS 5); (2b): mainly quartz conglomerates and microconglomerates fossiliferous with plane-parallel lamination (MIS5); (2c): polygenic gravels and sands alternating with fossiliferous horizons, to inclined lamination and foresets (MIS 5); (2d): bioclastic sandstone in *Lithtaminium* and bioconstructions in *Cladocora coespitosa*; (3a): limi sabbiosi palustri (MIS 4/2); (3b): silty sands with pulmonate gastropods (MIS 4/2); (4): bioclastic sandstone in *Cerastoderna sp* (Holocene); (5): polygenic gravel with sandy matrix (Holocene); (6): littoral sands and gravels (Holocene); (7): silty sands lagoon deposits with interbedded peat in *Posidonia oceanica* (present); (8): sandy littoral deposits (present).

Figure 5. (**a**) A view of the section of Sa Illetta marine interglacial fossiliferous sediments [8]; tidal plain sandy littoral deposit irregularly cemented with burrows bioturbation structures and plane-parallel lamination (Sections 1 and 2); (**b**) Section 2 bottom 2a, particular of the icnofacias due to the activity of *Polychaetes;* (**c**) Section 2 top 2d, bioclastic sandstone well cemented containing *Lithtaminium* and bioconstructions in *Cladocora coespitosa* -149 ± 10 kyrs BP [23]; (**d**) A view of the section of the last interglacial interdidal fossiliferous sediments of Is Arenas (Section 3, 2a) bottom level with burrows bioturbation structures containing *Persististrombus latus* [23]; (**e**) At the top conglomeratic heterometric and polygenic fossiliferous level (Section 3, 2b), at the bottom weakly cemented sandstones and sands with channeled flow structures in a tidal plane environment (Section 3, 2a); (**f**) sub-horizontal laminated sandstone enclosing a forest level containing *Arca Noae Limne, Arca tetragona tetragona Poli, Glycimeris sp*. 111 kyrs BP [35].

3.1.2. Oristano North Coastal Plains and Sinis Peninsula

An extensive wave-cut platform, incised in middle Miocene marlstone and upper Pliocene basalts, was detected in the eastern coast of Capo San Marco (southern part of the Sinis peninsula – Figure 6). The littoral deposit of MIS 5.5 is set on the platform, represented by a heterometric conlomerate with large basaltic blocks at the base, followed by micron-glomerates and plane-parallel lamination fossiliferous sandstone with *Persististrombus latus, Patella ferruginea, Mytilus galloprovincialis* up to the altitude of +4.5 m [36]. The inner margin,

generally hidden by MIS 5.5 littoral sediments and the overlying eolianites (MIS 4-2), is observable in the southernmost part of Capo San Marco at +6.5 m.

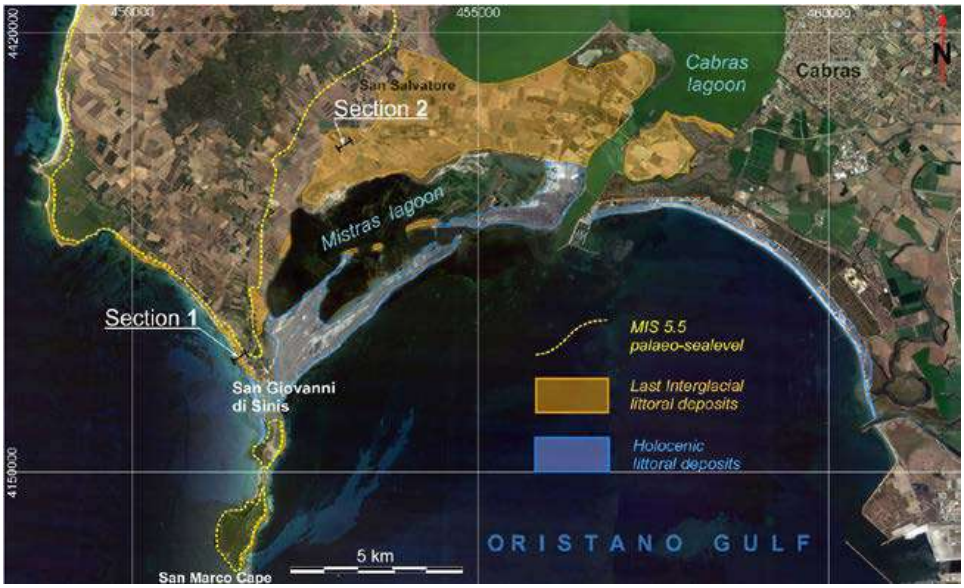

Figure 6. Aerial photograph of the coastal plain north of Oristano and the Sinis peninsula showing the main geomorphological features, yellow dashed line indicates the paleo high sea level of MIS 5.5; the littoral deposits of the last interglacial (LI) and the Holocenic shore deposits. Location of MIS 5 stratigraphic sections (Figure 7): Section 1 on the rocky coast of San Giovanni, Sinis peninsula; Section 2, on a Punic quarry located in the Cabras paleo-littoral barrier of MIS 5.

The MIS 5.5 marine-littoral deposits sequence is most preserved along the western coast of San Giovanni di Sinis [37].

The sequence (Figure 7, Section 1) is interrupted by erosion surfaces incised into the continental aeolian and colluvial deposits containing vertebrate and gastropod pulmonate remains from MIS 6. The transgressive succession is characterized from the base by polygenic erometric conglomerates, passing to fossiliferous quartz microconglomerates and fossiliferous sandstones (*Arca noae, Mytilus galloprovincialis, Spondylus gaederopus, Patella ferruginea, Thai haemastoma, Dentalium* sp.) with plane-parallel and inclined lamination (Figure 8).

The continuity of the sequence is interrupted by numerous erosion surfaces that sometimes retain levels or pockets of sandy paleosols with a strongly oxidized matrix. At the top, the MIS 5.5 sequence is sealed by continental deposits with sandy colluvium and aeolian sandstone cross-lamination (MIS 4-2).

The paleo-littoral bar of the MIS 5.5 that closes the Cabras lagoon is made up of flat-parallel and inclined sandstones that include foreset structures. The summit depositional surface of the MIS 5 deposits is located at altitudes between +4.30 and +4.50 m (Figure 8, Section 2). The significant sections are revealed on the walls of irrigation canals and of ancient Punic-Roman quarries between Cabras and San Salvatore. The inner margin of the maximum marine ingression of MIS 5.5 is masked by slope deposits and river sediments from the Holocene.

3.1.3. Olbia Gulf and Coastal Plains

MIS 5.5 deposits in the Olbia Gulf were first described by Segre [38], which indicated extensive outcrops of conglomerates and fossiliferous sandstones along the northern coast of Golfo Aranci and along the southern coast of Tavolara Island in front of Spalmatore Bay (Figure 9).

Here, the transgressive level with large heterometric blocks. both crystalline and carbonate rocks, fossilizes the wave-cut platform set on inequigranular Leucogranites. This

basal level is covered by a well-cemented biogenic calcarenite with high fossil content (*Conus mediterraneus, Conus vayssieri, Hexaplex trunculus, Cerithium vulgatum, Cerithium rupestre, Bittium reticulatum, Thais haemastoma, Columbella rustica, Arca noae, Barbatia barbata, Spondylus gaederopontaus, Patella ferruginea, Chama gryphina, Venus verrucosa, Chamelea gallina* and *Tapes sp*.) [39].

The marine-littoral sediment sequence is organized at levels and lenses of coarse gravels, alternating with fine-grained sediments up to a maximum height of +5.5 m (Figure 10, Section 1 and Figure 11). MIS 5.5 deposits are sealed upward by strongly cemented continental landslide deposits (MIS 4?).

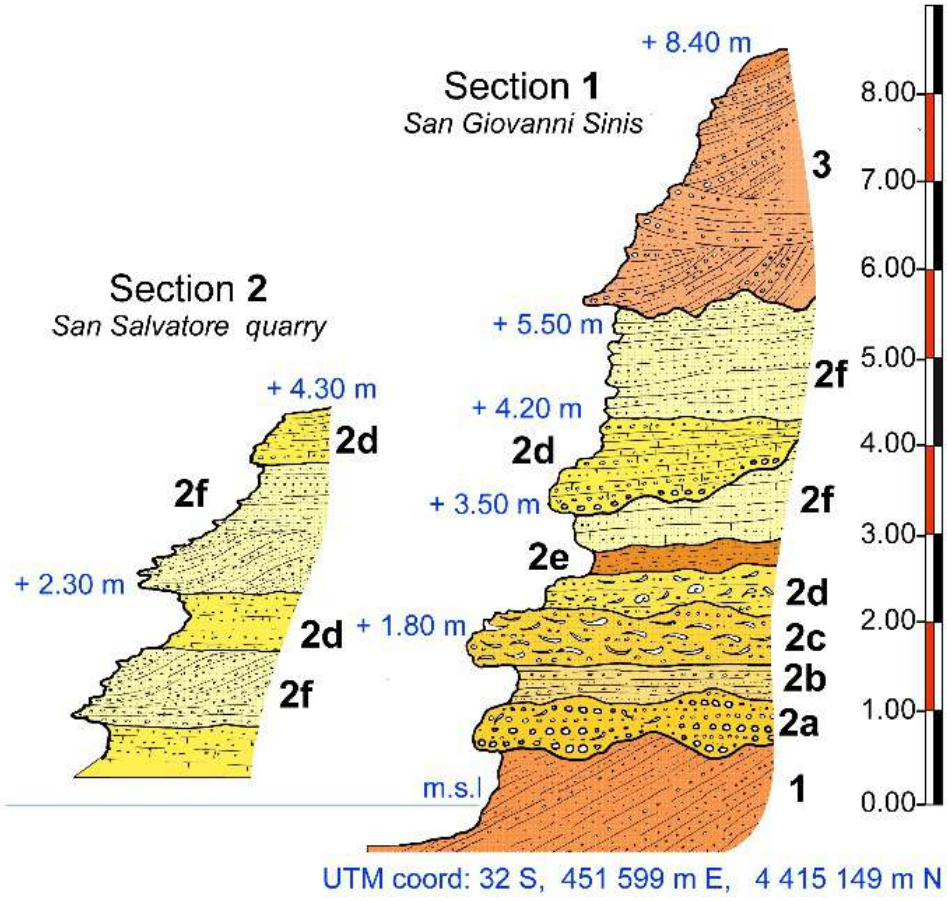

Figure 7. Stratigraphic sections of the medium-upper Pleistocene sequences in Oristano's north coastal plain and in the Sinis peninsula. (1) (Section 1): eolian sandstones with inclined layering laminae containing vertebrate remains (MIS6); (2a): polygenic heterometric conglomerate with a fossiliferous arenaceous matrix (MIS5); (2b): sandstones and micro-conglomerates mainly quartz with carbonate cement (MIS5); (2c): almost exclusively organogenic level in Mitilus galloprovincialis (MIS5); (2d): fossiliferous conglomerate and micro-conglomerates with a well-cemented arenaceous matrix (MIS 5); (2e): sandy palaeo-soil with a strongly oxidized matrix, Munsell 5YRS 5/8; (2f): planar-parallel lamination sandstones alternating with foreset levels (MIS5); (3): cross-laminated aeolian sandstones containing foraminifera and gastropods pulmonata Helicidae (MIS 4?) [36,37].

Figure 8. (**a**) DGPS measurements of the stratigraphic section of the Pleistocene deposits of San Giovanni of Sinis; (**b**) a view of the section of the San Giovanni stratigraphic showing continental deposits of the Middle Pleistocene and deposits of the last interglacial fossilized by regression aeolian sediments [8,36,37] (Figure 8); (**c**) particular of the organogenic level composed exclusively of valves of *Mitilus galloprovincialis* (MIS5); (**d**) excavation surface of the Phoenician-Punic quarry (2500 yrs BP) engraved in the MIS 5.5 beach sandstones in the paleo-littoral spit of Cabras; (**e**) detail showing the plane-parallel laminations that enclose a foreset level.

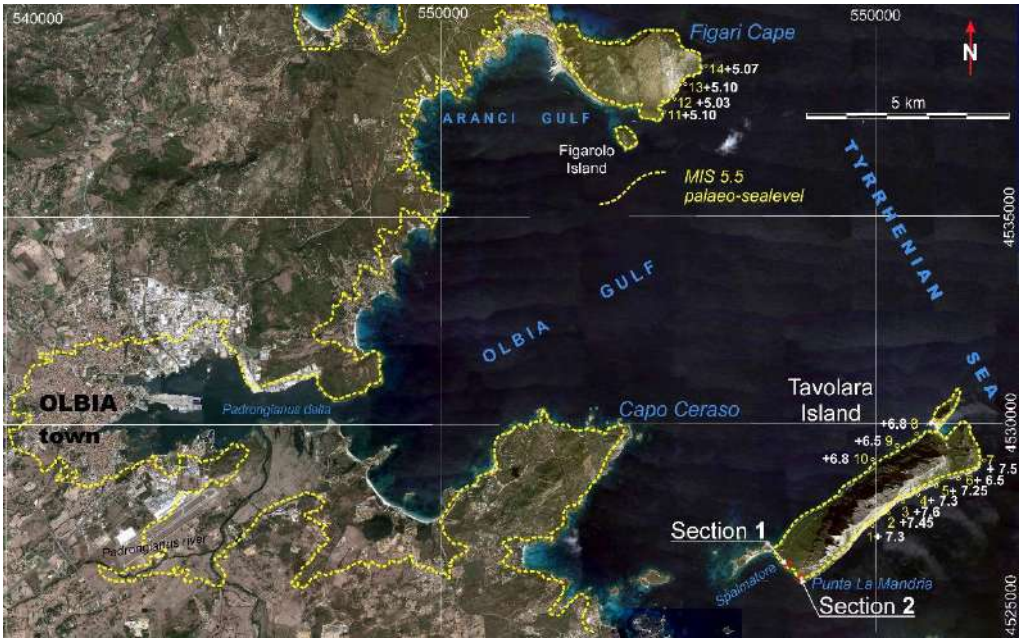

Figure 9. Aerial photograph of the coastal plain and the Gulf of Olbia, between the Figari Cape to the north and the Tavolara Island to the south, yellow dashed line indicates the paleo high sea level of MIS 5.5. Location of MIS5 stratigraphic sections (Figure 10): Section 1, on the Tavolara Island, east coast of the bay of Spalmatore. Section 2, near the promontory of Punta La Mandria, southernmost point of the Tavolara Island and elevations of the tidal notch of the MIS 5.5 [39].

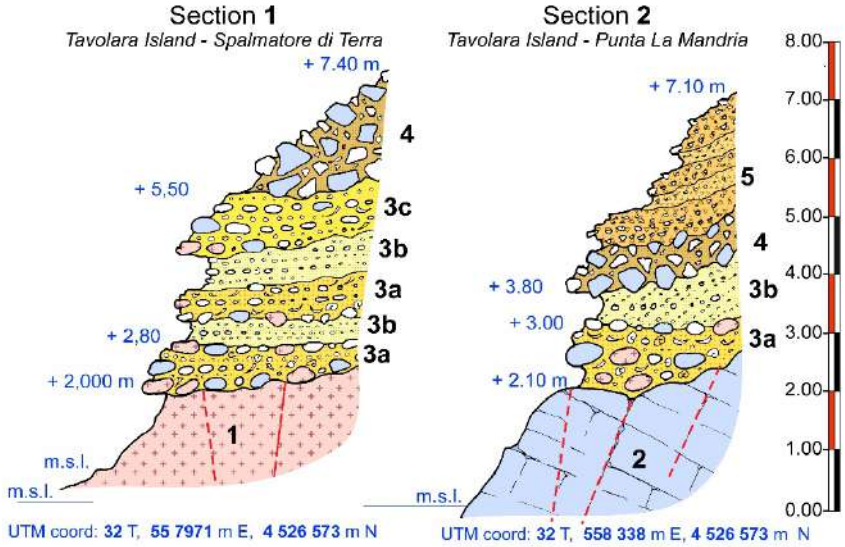

Figure 10. Stratigraphic sections of the MIS 5.5 littoral deposits in Tavolara Island, in front of the Olbia coastal plain. (1): Section of Spalmatore Baya (Section 1), inequigranular medium-grained pink leucogranites with phenocrysts of quartz and K Feldspars (Upper Carboniferous). (2) Section of Punta La Mandria (Section 2), dolomite arenaceous, dolomitic limestone from coasts to circalittoral, with foraminifera and red algae (Dorgali Formation, Middle Jurassic). (3a) Polygenic heterometric conglomerate with alternating quartz micro-conglomerates in fossiliferous arenaceous matrix (MIS 5); (3b) sandstones and micro-conglomerates mainly quartz, fossiliferous with plane-parallel and foreset lamination (MIS5); (3c) heterometric conglomerate of granite and dolomite blocks, in an arenaceous matrix with carbonate cement. (4) Well-cemented landslide deposit (MIS 4-3?). (5) Deposit of stratified slope with alternations of Eboulis ordonnés and Grezes litees (LGM-MIS 2).

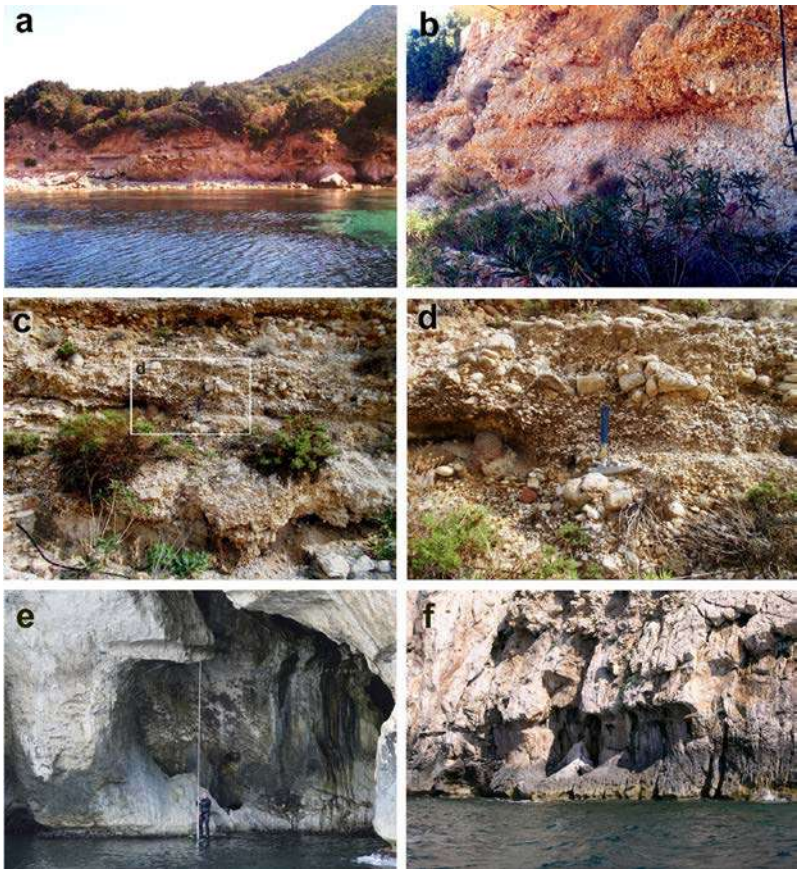

Figure 11. (**a**) A view of the section of Spalmatore Bay marine interglacial fossiliferous sediments transgressive on the granite substrate, Section 1 [8,38,39]; (**b**) conglomeratic heterometric and polygenic fossiliferous level at the bottom weakly cemented sandstones in parallel-plane lamination; (**c**) section of Punta La Mandria (Section 2) heterometric conglomerate in an arenaceous matrix with a high fossil content resting on a surface of irregular erosion engraved in the dolomitic limestones of Punta La Mandria; (**d**) detail of the previous image, of the conglomerates and micro-conglomerates containing the remains of gastropods (*Patella ferruginea, Verithium vulgatum; Cipraea lurida*) e lamellibranchi (*Spondilus gaederopus; Mitililus galloprovincialis, Arca noae; Venus verrucosa*); (**e**) tidal notch at +7.5 m in the northeastern sector of the Island of Tavolara, Grotta del Papa, altitude measurement through a precision telescopic staff; (**f**) tidal notch (2) at +7.3 m in the eastern sector of the Island of Tavolara. Part of the continental deposit can be seen at the base, aeolian sandstones at the base and on the slope at the top that fossilized the MIS 5 paleo-tidal notch.

The sedimentary sequence of MIS 5.5 at Punta La Mandria has a lower thickness and rests discordantly on both Paleozoic granitoid substrate and Middle Jurassic arenaceous dolomitic limestone. The succession is fossilized by both rockfalls and cryoclast deposits represented by alternating Eboulis ordonnés and Grezes litees (LGM).

Data about the elevation of tidal notches incised during the MIS 5.5 highstand are presented. The elevations (Figure 10, Table 2) show a relative tectonic stability of the area, but a slight negative tilting; differing the elevations of the southern cliff to the northern cliff of Tavolara Island. This tendency is more marked towards Capo Figari.

Similar movements, although of greater magnitude, have been found in the Gulf of Orosei and Capo Caccia [7].

3.2. Geomorphology and Altitude of MIS 5.5 Transgression in Pontina Plain

Located in Italy, south of Rome, the Pontina Plain is bordered to the north by volcanoes and pyrso-clastic deposits of Albani hills, to the east by the Lepini and Ausoni mountains (Mesozoic carbonates complexes) and to the west by the Tyrrhenian Sea (Figure 12). This

area is characterized by a distensive tectonic regime, that was active during the Pliocene and the Quaternary, linked with the tectonic opening of the Tyrrhenian Sea. In this context, the Pontina Plain represents a sector of particular geological complexity, as the interaction of the sea level changed with neotectonic phenomena.

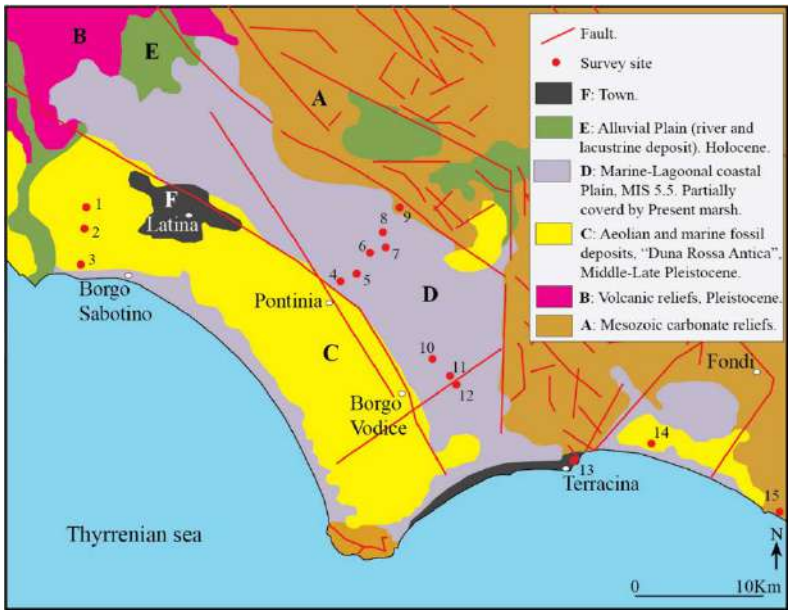

Figure 12. Main geological outcrops of the Pontina Plain, this map is a compilation of: (i) Italian Geological Survey sheet numbers 170, 158 and 159; (ii) map of the soil [40]; (iii) sinkhole map of Regione Lazio http://www.regione.lazio.it/binary/rl_main/tbl_documenti/AMB_PBL_Carta_Sinkholes_Lazio_2011.pdf accessed on 20 June 2021. The red dots refer to the sites described in Table 3.

Table 3. On this table all the outcrops dated to MIS 5.5 found studied in the Pontina Plain from Borgo Sabotino (NW) to the Piana di Fondi (SE) and the carbonate promontories of Sperlonga and Gaeta are listed (Figures 13 and 14). In particular, for the lagoon facies sites found in Section D of Figure 12 and published in [20] (Pontinia and Borgo Vodige), an infield check was carried out with respect to the presence of fossil deposits, their share and the fossiliferous association. Section E shows images of channels in the silty portion of the Pontina and Fondi Plain. The flow of the springs in conjunction with moments of high tide can lead to the deposition silts that are flooded and sometimes partially cover the MIS 5.5 fossil lagoon that extends inland for tens of kilometers.

	A	B	C	D	E	F
n.	**Site**	**Coordinates**	**MIS 5.5 Altitude (m)**	**Kind of Marker**	**Age**	**References**
1	Fosso Moscarello Gnif Gnaf, Santa Maria	41.4615 12.8112	10 ± 1	Fossil beach containing *Persistrombus latus*	Senegalese Fauna Aminoacid	[41,42]
2	Canale Mussolini	41.4483 12.8107	5.1 ± 0.1	Fossil beach containing *Persistrombus latus*	Senegalese Fauna Aminoacid	[39,43,44]
3	Nuclear power plant Borgo Sabotino	41.4231 12.8053	−4.3 + 5 ± 0.5	Fossil beach containing *Persistrombus latus*	Senegalese Fauna	[44]
4	Pontinia 1	41.4129 13.0449	+5.3 ± 0.5	Lagoonal facies with *Cerastoderma* sp.	Geomorphological correlation	[20,45]
5	Pontinia 2	41.4172 13.0600	+4.4 ± 0.5	Lagoonal facies with *Cerastoderma*	Geomorphological correlation	[20,45]
6	Pontinia 3	41.4323 13.0721	+2.3 ± 0.5	Lagoonal facies with *Cerastoderma* sp.	Geomorphological correlation	[20,45]

Table 3. *Cont.*

	A	B	C	D	E	F
n.	**Site**	**Coordinates**	**MIS 5.5 Altitude (m)**	**Kind of Marker**	**Age**	**References**
7	Pontinia 4	41.4355 13.0864	+0.8 ± 0.5	Lagoonal facies with *Cerastoderma* sp.	Geomorphological correlation	[20,45]
7.1	Check in field	41.434771 13.062667	−1 ± 0.5	Cerastoderma e Tapes, travertino con incrostazioni	Geomorphological correlation	This paper
7.2	Check in field	41.3757510 13.1281060	−2 ± 0.5	Lagoonal facies with *Cerastoderma* sp.	Geomorphological correlation	This paper
7.3	Check in field	41.363875 13.140631	−3 ± 0.5	Lagoonal facies with *Cerastoderma edulis*, *Tapes decussatus*, *Nassa mutabilis*	Geomorphological correlation	This paper
8	Pontinia 5	41.4424 13.0751	−0.5 ± 0.5	Lagoonal facies with Cerastoderma	Geomorphological correlation	[20,45]
9	Mezzaluna core	41 27 47 13 06 01	−14.30 − 11.41 ± 0.5	Venus and Cerastoderma	Pollen Analysis, U\Th and aminoacid	[46]
10	Borgo Vodige 1	41.3571 13.1317	1 ± 0.5	Lagoonal facies with Cerastoderma	Aminoacid	[20,45]
11	Borgo Vodige 2	41.3497 13.1293	−0.6 ± 0.5	Lagoonal facies with Cerastoderma	Aminoacid	[20,45]
12	Borgo Vodige 3	41.350 13.117	−1.80 ± 0.5	Lagoonal facies with Cerastoderma	Aminoacid	[20,45]
13	Terracina	41.288 13.260	7.96 ± 0.1	Tidal notch	Geomorphological correlation at 5 km from aged MIS 5.5 deposit	[7]
14	Fondi APT4	41.0065 13.331	−6\−24	Marsh with Cerastoderma Aminozone E	Aminoacid	[47]
15	Sperlonga	41.229691 13.502001	7.30 ± 0.5		Geomorphological correlation	[8]
16	Sperlonga	41.2187 13.5321	6.53 ± 0.1	Tidal notch	Geomorphological correlation	[47]
17	Gaeta	41.2046 13.5774	5.92 ± 0.1	Tidal notch	Geomorphological correlation	[47]

Forms and deposits aged MIS 5.5, in particular fossil tidal notches and *Cerastoderma* living in lagoons, are considered the best markers to detect even small vertical tectonic movements occurred during the last interglacial [7,8]. As regards the research and studies published for the Quaternary (Upper Pleistocene) of the Pontina Plain, they began in the 1930s and continued until 2018 with the study, analysis and dating of new fossil deposits, cores or fossil tidal notches [7,20,39,43–51].

We can divide the Pontina Plain into two completely different geomorphological areas: a sandy aeolian portion called Duna Rossa [52] with developed paleosols that preserved erosion and morphology which extends from the Tyrrrhenian Sea coast up to about half of the Pontina Plain (with altitudes between 15 and 30 m); and a silty peaty portion (subject to strong compaction starting from the 1930s) with altitudes reaching 5 m to the north and up to −3 m to the south near the carbonatic mountains. The negative altitudes are due to: (i) extensive subsidence phenomena caused by the drying of peat up to over 6 m [53]; (ii) sinkhole phenomena in the Pontina Plain eastern portion near the contact with Mesozoic carbonates; (iii) possible direct fault actions that lower the Mesozoic carbonates under the Pontina Plain (Figure 12). The lower elevation portion of the plain is towards the eastern portion which is bordered by the Lepini mountains (Mesozoic Carbonates) which, with direct faults, "descend" under the plain; towards the west it borders the formation of the Duna Rossa, aeolian sands aged from the Middle Pleistocene, MIS 5.5, MIS 4, 3 and 2. These

deposits are engraved to the north by some reclamation drainage channels including (at Borgo Sabotino) the "Mussolini channel", whose excavation allowed the *Persistrombus latus* findings [8,45] to place them at +10 m; however, after a careful reading of the original paper by the authors of [54] we can conclude that the highest deposits of the central/southern Pontina Plain containing *Persistrombus latus* are located at +5.3 m, the northern portion, near Rome. Blanc, in 1957, performed at Canale Mussolini, one of the first radiocarbon ages of Europe, dating the deposits as older than MIS 5.5: wood and peat, attributing them to MIS 4. In the higher levels, the authors of [55] published an interesting mammalian fauna with *Megaloceras, Equus idruntinus, Ursusu speleus*. On the depressed peaty area of the Pontina Plain (Figure 13, Figure 14), the MIS 5.5 deposits dated with aminostratigraphy [20] were found between +3 m to −2 m. These negative altitudes, often present in the Pontina (up to −4 m) derive in part from the reclamation that has left up to 16 m [53] of peat which causes drying to produce a considerable subsidence, especially in correspondence with some areas (former sinkholes) close to the limestones of the Lepini-Ausoni mountains.

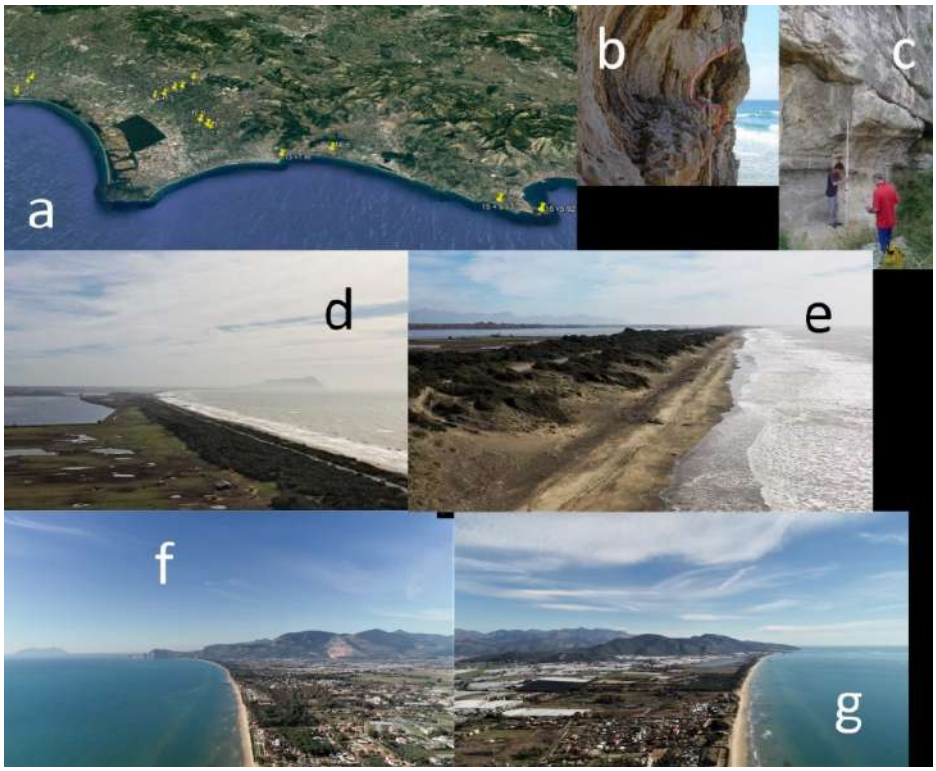

Figure 13. (**a**) Google Earth image of the Pontina and Fondi Plain with the carbonatic promontory of Terracina, Sperlonga on which are carved the fossil tidal notches; (**b**,**c**) aged MIS 5.5, the yellow arrow indicates the sample's number and altitude (see Table 3) Pianura Pontina e di Fondi; (**d**) the coastal area of northern Pontina Plain (on background, the limestone Circeo promontory); (**e**) the coastal area of northern Pontina Plain (on background, the limestone Terracina promontory; (**f**) the coastal area of the Fondi Plain (on background, the limestone Terracina Promontory; (**g**) same point but a southern view, with Sperlonga promontory.

Figure 14. (**a**) *Cerastoderma edulis* sampled in a section outcropping in the channel of this figure in (**e**); (**b**) *Tapes decussatus* from the outcrop on the reclamation drainage c channel; (**c**,**e**) the channel (**d**), the Mussolini channel during the excavation in the 1930s; (**f**) *the outcrop Nassa mutabilis Tapes decussatus, Cerastoderma edulis;* (**f**) a fossiliferous level very rich in lagoon fauna. See also Table 3 site 7.1.

3.3. Maps of the Pontina Plain

On the basis of the maximum altitude of the highstand reached during the MIS 5.5 of 8.2 m, [47] and the present altitude of the Pontina Plain maps (Table 1), it was possible to reconstruct the transgressive event that occurred 119 ka BP: a gulf that forwards in a NW direction for about 32 km, with a total flooded area of 401.42 km^2 (Table 4) and about 100 km of coastline involved in the transgression of 119 ka BP (Table 2). This high sea stationing event is demonstrated by the data (forms and deposits) emerging in the plain and described in the previous chapter. Based on the IPCC 2019 data, in 2300 the maximum elevation of the sea will be 5.249 m higher than in 2019. Based on the elevation of the Pontina Plain maps it was possible to reconstruct the possible future transgressive event (Figure 15), provided that "man" does not carry out any anthropic building (dams, genic interventions (dams, water pumps, etc.). Figure 15 shows a gulf that will extend into the Pontina Plain for about 26 km and that could have a total flooded area of 306.67 km^2.

Table 4. A: coastal sites; B: exposure; C: maximum fetch; D: max fetch; E: coastal material; F: wave energy flux kW\m. This is an average between two types of data in [56]. Maximum waves and energy are found between the Balearic Islands and Capo Caccia with values between 9 and 10.0.; G: geomorphology; H: flooded area during MIS 5.5 km^2; I: projection flooded area IPCC 2300, km^2; L: projection flooded area IPCC 2100 km^2. As regards the flooded area of the Pontina Plain on the map (Figure 13), * we divided it into three different areas (Pontina 190, Fondi 64.5 and Laghi Costieri 49.2; M: exposed coastline Length km; N: human-made structures.

A	B	C	D	E	F	G	H	I	L	M	N
Site n°	Coastal Site	Exposure Direction	Max Fetch Km	Coastal Material	Wave Energy Flux kW/m	Geomorphology	Flooded Area MIS 5.5 km^2	Flooded Area IPCC 2300 km^2	Flooded Area IPCC 2100 km^2	Exposed Coastline Length km	Human-Made Structures
1	Pontina Plain *	N-W	308	sand	3–4	Embayed Beach	396.3	303.7	61	104.9	Towns and Agricultural crops
2	Cagliari	S	208	sand	4–5	Barrier and lagoon systems	131.5	87.2	27.5	29.6	Towns and Agricultural crops
3	Oristano	W	357	sand	6–7	Barrier and lagoon systems	376.8	230.0	53.5	102.7	Towns and Agricultural crops
4	Olbia	E	231	sand	3–4	Rias + Barrier and lagoon systems	24.7	16.3	4.53	30.7	Towns, harbor and industrial hub

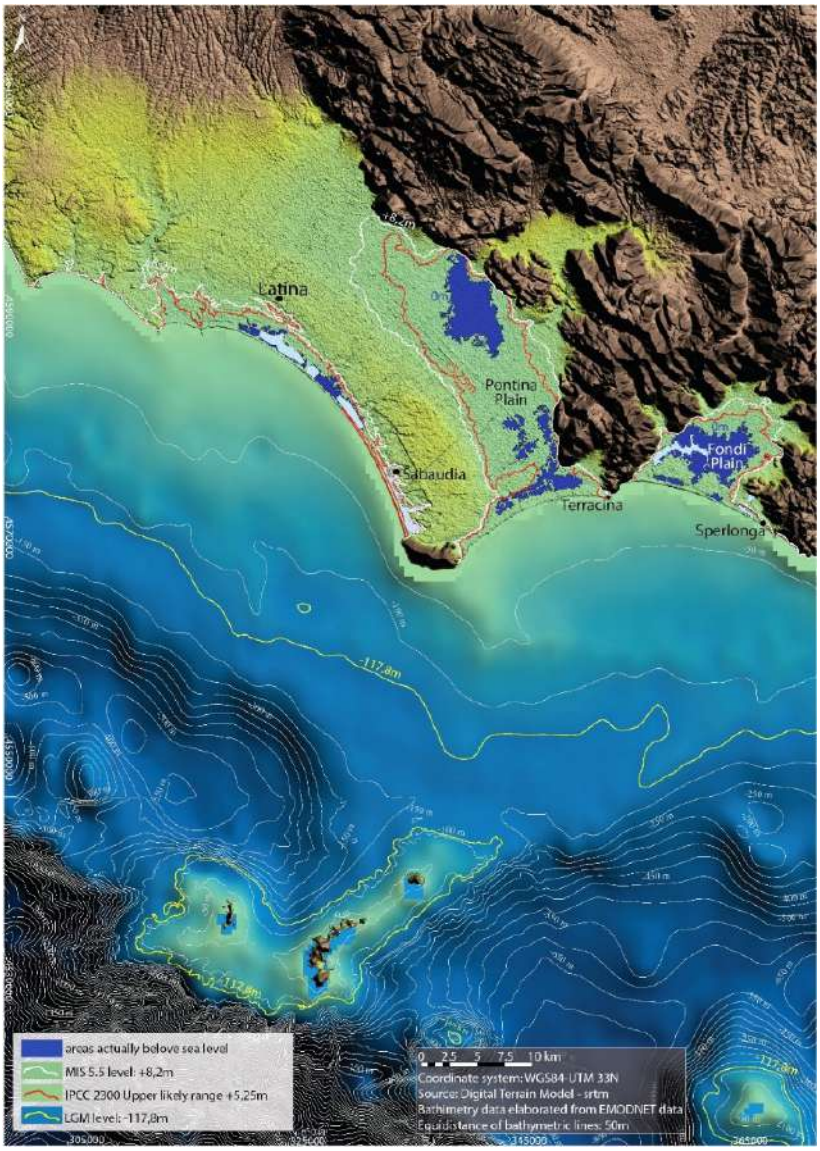

Figure 15. The Pontina and Fondi Plains maps showing the potential submersion area using IPCC AR5 RCP 8.5 for 2100 and 2300: the MIS 5.5 extension occurred 119 ka BP.

3.4. Maps of Cagliari Plain

The northern sector of the Gulf of Cagliari is characterized by a flood plain with a low slope towards the south. In this sector, during MIS 5.5, the maximum altitude of +8.4 m above current sea level originated two bays: one to the west (current Laguna di Santa Gilla) with a retreat of the shoreline of about 16 km and one to the east (current Molentargius) with 6 km of retreat. The Sant'Elia promontory was isolated from the mainland and represented an island or was probably connected to the coast through a tombolo. The map shows that in MIS 5.5, the marine transgression affected the coastal sector wide 27 km with a flooded area of 131.54 km^2. The same map shows the maximum level of + 5.25 m compared to the sea level for the year 2300 based on IPCC 2019 data; in particular, the map shows a scenario which 87.24 km^2 of coastal areas submerged; the sea level rise would lead to the demolition of the Holocene littoral spits with a shoreline retreat of 16 km and 14 km, respectively, for the Santa Gilla and Molentargius lagoons and the subsequent formation of bay beaches (Figures 16 and 17).

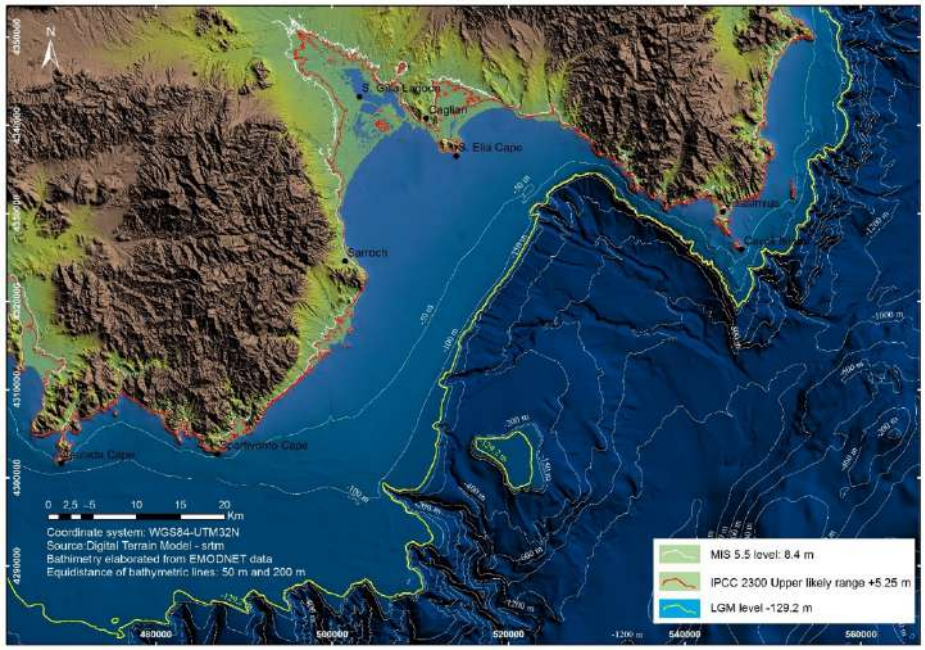

Figure 16. The Cagliari plane map showing the potential submersion area using IPCC AR5 RCP 8.5 for 2100 and 2300: the MIS 5.5 extension occurred 119 ka BP.

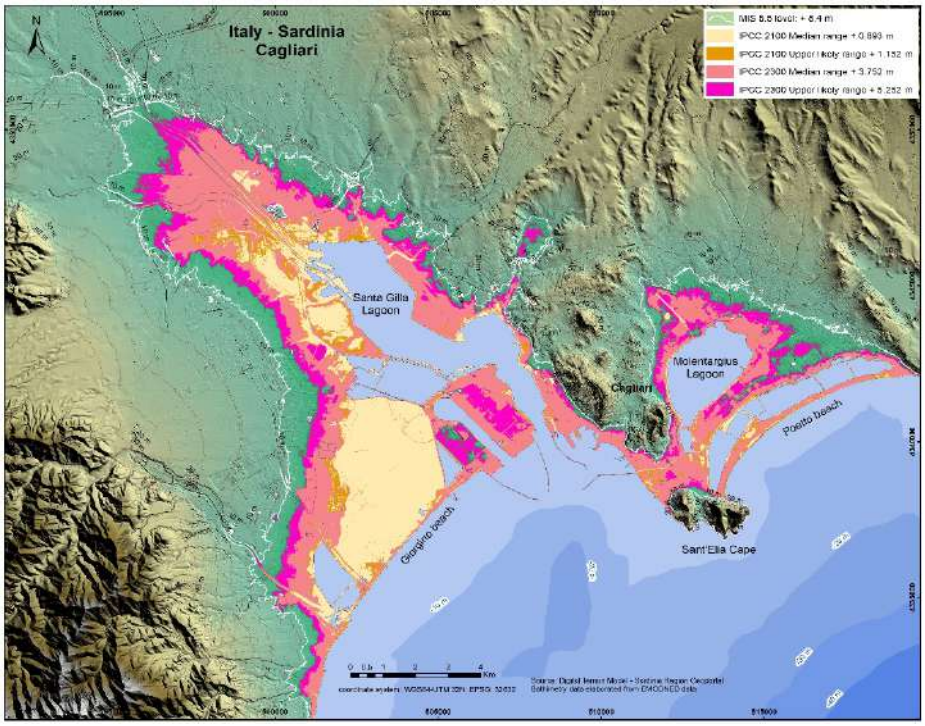

Figure 17. Map of Cagliari plane, (see also Figure 2 for location). The potential submersion area, using IPCC AR5 RCP 8.5 projections at 2100 and 2300.

3.5. Maps of Oristano Plain

In the Gulf of Oristano, the MIS 5.5 shoreline reaches a maximum level of +8.5 m a.s.l. In addition, for this sector the slope is very low; there is a maximum shoreline retreat of about 13 km and a submersion area of about 376.77 km^2. The map shows the maximum level of +5.25 m above sea level for the year 2300 based on IPCC 2019 data. This scenario would lead the demolition of the Cabras and Santa Giusta littoral spits, the submersion of

230 km^2 in a sector of coastline that extends for 103 linear km and the retreat of the Tirso River mouth towards the northeast (Figures 18 and 19).

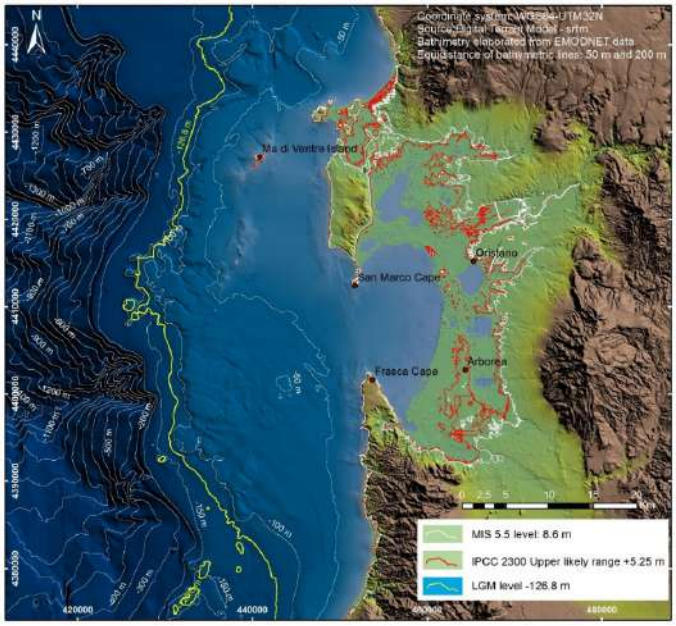

Figure 18. The Oristano plane map showing the potential submersion area using IPCC AR5 RCP 8.5 for 2100 and 2300: the MIS 5.5 extension occurred 119 ka BP.

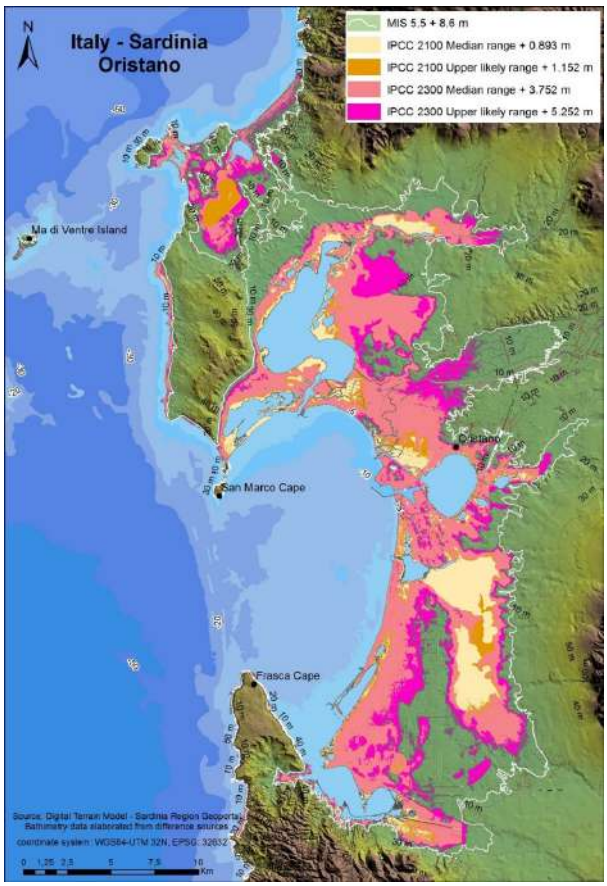

Figure 19. Map of Oristano plane, (see also Figure 2 for location). The potential submersion area, using IPCC AR5 RCP 8.5 projections at 2100 and 2300.

3.6. Maps of Olbia Plain

The Gulf of Olbia is represented by a rias coast engraved on granite lithologies. The slopes are greater than the alluvial plains of Cagliari and Oristano. For this reason, the MIS 5.5 sea level with an altitude of +8.5 m a.s.l. was measured up to a maximum of 2 km from the current shoreline, while the submerged surface during MIS 5.5 was equal to 24.69 km^2. For this area, the sea level on the basis of the IPCC 2019 data will reach the maximum altitude of +5.25 with the submersion of 16.31 Km^2 of coastal area. The map shows the demolition of the lagoon behind Le Saline beach, the retreat of the Rio Padrongianus mouth and the retreat of approximately 1 km in correspondence of the city of Olbia (Figures 20 and 21).

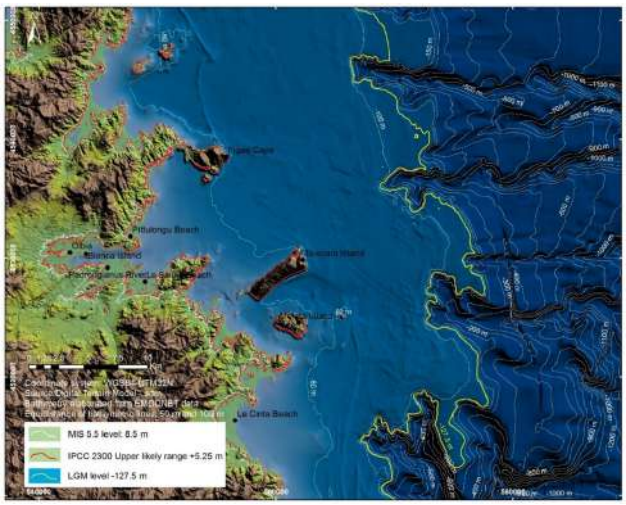

Figure 20. Olbia plane map showing the potential submersion area using IPCC AR5 RCP 8.5 for 2100 and 2300: the MIS 5.5 extension occurred 119 ka BP.

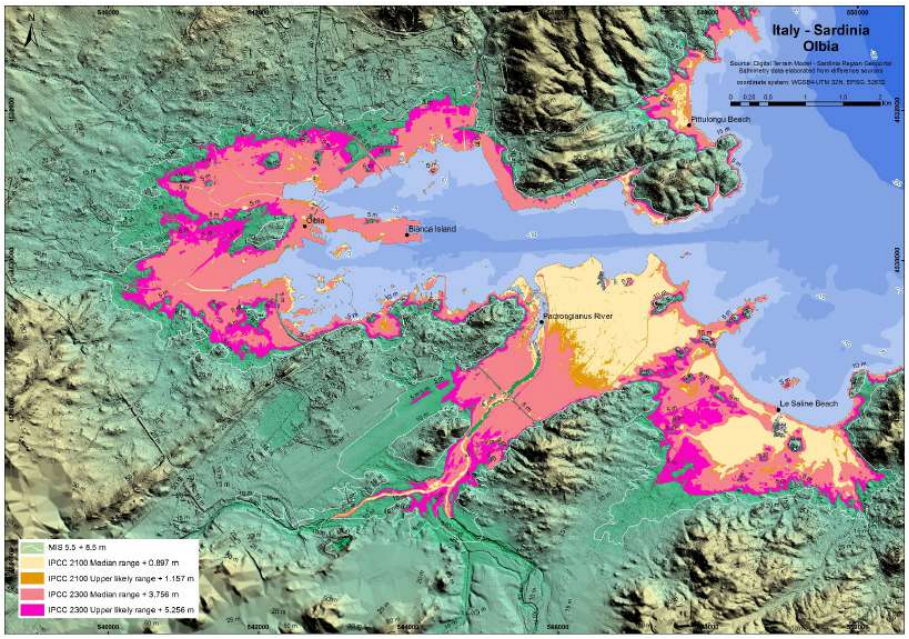

Figure 21. Map of Olbia plane, (see also Figure 2 for location). The potential submersion area, using IPCC projections at 2100 and 2300.

4. Discussion

The paleo-climatic events that 125 kyrs BP have led to a notable ice melting with a global consequence of a sea level rise more than 5–7 m around the world, are still the

subject of scientific debate. With regard to the CO_2 content in the atmosphere, 119 ka BP, was considerably lower than today, but the insolation was higher. In fact, such a high sea level (and carbon dioxide in the atmosphere) was never reached except in the Pliocene [57]. Gilford et al. 2020 [58] explore the extent to which MIS 5.5 constraints could inform future Antarctic contributions to sea level rise, forcing the last interglacial with IPCC RCP8.5, and obtaining a sea level over year 2150 of about 5 m even beyond the 2019 IPCC forecasts.

As regards data and interpretations on insolation, due to astronomical variables dynamics they are not univocal and are difficult to compare with each other due to the different measurement methods and sensors [59,60]. Data sets of daily SSR records (1953–2013) were interpolated on a regular grid and grouped into two regions, northern and southern Italy, both in all-sky and clear-sky SSR mode [61].

While taking into account the IPCC literature which mainly indicates a phase of decrease in insolation in the last 6 Ka, the warming recorded in the last two centuries is due to the increase in CO_2 (IPCC 2019).

The possibility is also considered that, on the contrary, there is an increase in the insolation of an astronomical origin (Milankovic cycles) characteristic of an interglacial phase [62,63], a condition that finds support in the data from geo-archaeological indicators of the last 4 Ka [33]. In this case, the increase in CO_2 would contribute to global warming by accelerating the upward trend of the sea level [1].

For all these reasons, we think that the approach of using the maximum transgression occurred for 119 ka BP has serious scientific motivations. None of the authors are hoping for a sea level rise above 1 m in 2100, but in light of what happened during MIS 5.5 it seemed useful to have a realistic view of the effects. The maximum altitude that sea level reached during MIS 5.5 can therefore be considered as a reference also for future sea level rise.

4.1. Pontina Plain

The Pontina Plain map (Figure 15) highlights a long paleo-gulf that falls for 33 km. It should also be emphasized that the eastern portion of the Pontina Plain is subject to a subsidence partly induced by the reclamation, by partial drying of the peat and partly to negative tectonic movements, especially in correspondence with the eastern edge of the Pontina Plain in contact with the Mesozoic Carbonate. In some areas of the Pontina Plain, we found lagoonal deposits containing Cerastoderma edulis outcropping in field down to −2 m; these circumstances confirm small but continuous negative vertical movements especially in the southern portion of the Pontina Plain (Figure 15).

4.2. Sardinia

4.2.1. Cagliari Coastal Plain

The map of the Cagliari Coastal Plain highlights two deep inlets separated by the high structural system of the Cagliari hills—Cala Mosca-Sella del Diavolo promontory. The eastern inlet gave rise to the Molentarigius paleo-lagoon, closed by the littoral spit of Is Arenas (Figures 3 and 5, Section 3). In the sector of maximum expansion of the last interglacial transgression, strips of the inner margins engraved in MIS 6 alluvial deposits have been preserved (Figure 5, Section 4).

The western bay deepens into the plain for about 15 km. The MIS 5.5 transgression internal margin presents a marine terrace at Cerastoderma glaucum [28], from which a strip was found at +3.40 m (Figure **??**, Section 5). The coastal paleo-spit marine deposits of Sa Illetta, which closed the paleo-lagoon of Santa Gilla, were found up to an altitude of +4.30 m, while in correspondence of the two lagoon paleo-mouths of the MIS 5 fossiliferous levels are found at −2 m (east lagoon-mouth) and −5 m (west lagoon-mouth—La Plaja coastal spit).

4.2.2. Oristano–Sinis Coastal Plain

In the sector of Oristano, the last interglacial transgression entered in the coastal plain of Cabras for about 10 km, and no inner margin was clearly detected as it is covered by

river and slope deposits. A paleo-spit closes the paleo-lagoon of Cabras (Figure 6) with littoral sediments detected up to an altitude of 4.30 m (Figure 8, Section 2).

The maximum altitude of the littoral deposits of MIS 5 was found in San Giovanni di Sinis where sandstone with plane-parallel lamination reaches +5.50 m (Figure 8, Section 1), while on the eastern coast of the di Capo San Marco promontory an abrasion platform engraved in the Pliocene basalts with an inner margin at an altitude of +7 m is present.

4.2.3. Olbia Coastal Plain and Tavolara Island

The littoral deposits of the Olbia coastal plain were extensively studied by Aldo Segre in 1954. The significant increase in tourist construction on the coast during about 70 years has obliterated most of the outcrops that have instead been preserved on the Tavolara Island (for decades, a national marine protected area) (Figure 9).

The upper limit of the last interglacial is well marked in the area by tidal notches, at +7.5 m at Grotta del Papa (Figure 11e).

The MIS 5 fossiliferous deposits of Spalmatore di Terra (Tavolara Island), in high energy facies (conglomerates and micro-conglomerates) reach +5.5 m (Figure 11, Section 1).

Fossil deposits similar to those of MIS 3 were crossed by geotechnical cores at an altitude of −4 m in the area of the inner port of Olbia, a port area located in the bottom of the bay set on a deep Ria with a tectonic setting.

After the submission of the manuscript, the IPCC AR6 report was published. This report confirms and studies in depth the previous report (AR5) and also enters into the merits of particular areas such as the Mediterranean. The AR6 report provides, for example, the relative sea level rise of the Mediterranean expected in 2100 in numerous coastal locations, including Cagliari, one of our four sites. As can be seen in Figure 22 from the report released 10 days ago, the forecasts for the RCP8.5 scenario used by us are very close to what we reported in Table 1 for Cagliari. The IPCC value is 0.78 ± 0.3 m; the value used by us for Cagliari for 2100 in Table 1 is 0.89 m.

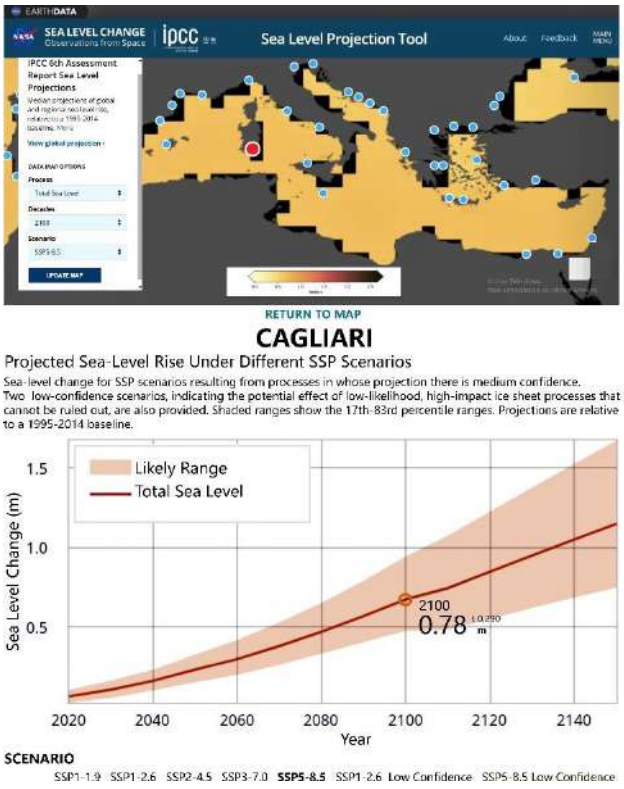

Figure 22. Projected Sea Level Rise of Cagliari coastal plane after IPCC AR6 [18]—https://sealevel.nasa.gov/ipcc-ar6-sea-level-projection-tool. (accessed on 28 August 2021).

5. Conclusions

In this work, we have shown a methodology to create precise maps with potentially expected submersion scenarios for 2100 in four selected coastal zones of the Mediterranean basin which are prone to marine submersion under the effects of relative sea level rise. For these areas, we produced thematic maps that were based on climatic scenarios, tectonics, local geological behavior and the best available digital topography.

Some areas are natural high value sites belonging to protected areas or national parks; some are deeply urbanized by residential or touristic settlements; others are characterized by the presence of cultural heritage, and infrastructure such as communication routes and harbors.

From our analysis, we estimated that during MIS 5.5, the whole studied sites were flooded by the sea at an area of 929.3 Km^2: 396.3 Km^2 in the Pontina Plain, 131.5 Km^2 in the Cagliari Plain, 376.8 for Oristano Plain and 24.7 for the Olbia Plain. The potential loss of land for the above areas in 2300 are 146.5 Km^2, and in 2100 are 146.5 Km^2 for the IPCC-RCP8.5 whole sites studied, impacting a coastline length of about 267.9 km. In these coastal areas are often located densely inhabited settlements and infrastructure. The expected scenario and the exposition of the investigated areas to coastal hazards should be considered for cognizant management of the coastal zone.

The comparison between the maximum ingression line of the last interglacial and the present evolutionary trend of submersion of the coastal plains is justified by the fact that, at the current state of knowledge, it cannot be excluded that the maximum altitude the sea level reached during MIS 5.5 can therefore be considered as a reference also for the future sea level rise.

Author Contributions: Conceptualization, G.D., F.A., P.E.O. and V.L.P.; methodology, G.D., F.A. and V.L.P.; software, G.D., L.M. and V.L.P.; validation, F.A. and P.E.O.; formal analysis, G.D., F.A., P.E.O. and V.L.P.; investigation, G.D., F.A., P.E.O. and V.L.P.; resources, G.D., F.A., P.E.O. and V.L.P.; data curation, G.D., G.R. and V.L.P.; writing—original draft preparation, G.D. and V.L.P.; writing—review and editing, G.D., F.A., P.E.O. and V.L.P.; visualization, G.R.; supervision, F.A. and P.E.O.; project administration, G.D., F.A., P.E.O. and V.L.P.; funding acquisition, F.A. and P.E.O. All authors have read and agreed to the published version of the manuscript.

Funding: This research received no external funding.

Institutional Review Board Statement: Not applicable.

Informed Consent Statement: Not applicable.

Data Availability Statement: Data is contained within the article.

Conflicts of Interest: The authors declare no conflict of interest.

References

1. Vacchi, M.; Joyse, K.M.; Kopp, R.E.; Marriner, N.; Kaniewski, D.; Rovere, A. Climate pacing of millennial sea-level change var-iability in the central and western Mediterranean. *Nat. Commun.* **2021**, *12*, 4013. [CrossRef] [PubMed]
2. Lambeck, K.; Antonioli, F.; Anzidei, M.; Ferranti, L.; Leoni, G.; Scicchitano, G.; Silenzi, S. Sea level change along the Italian coast during the Holocene and projections for the future. *Quat. Int.* **2011**, *232*, 250–257. [CrossRef]
3. Antonioli, F.; Anzidei, M.; Amorosi, A.; Presti, V.L.; Mastronuzzi, G.; Deiana, G.; De Falco, G.; Fontana, A.; Fontolan, G.; Lisco, S.; et al. Sea-level rise and potential drowning of the Italian coastal plains: Flooding risk scenarios for 2100. *Quat. Sci. Rev.* **2017**, *158*, 29–43. [CrossRef]
4. Marsico, A.; Lisco, S.; Presti, V.L.; Antonioli, F.; Amorosi, A.; Anzidei, M.; Deiana, G.; De Falco, G.; Fontana, A.; Fontolan, G.; et al. Flooding scenario for four Italian coastal plains using three relative sea level rise models. *J. Maps* **2017**, *13*, 961–967. [CrossRef]
5. Bonaldo, D.; Antonioli, F.; Archetti, R.; Bezzi, A.; Correggiari, A.; Davolio, S.; De Falco, G.; Fantini, M.; Fontolan, G.; Furlani, S.; et al. Integrating multidisciplinary instruments for assessing coastal vulnerability to erosion and sea level rise: Lessons and challenges from the Adriatic Sea, Italy. *J. Coast. Conserv.* **2019**, *23*, 19–37. [CrossRef]
6. Pörtner, H.O.; Roberts, D.C.; Masson-Delmotte, V.; Zhai, P.; Tignor, M.; Poloczanska, E.; Mintenbeck, K.; Nicolai, M.; Okem, A.; Petzold, J.; et al. (Eds.) *IPCC, 2019: Special Report on the Ocean and Cryosphere in a Changing Climate*; Cambridge University Press: Cambridge, UK; Cambridge University Press: New York, NY, USA, 2019.

7. Antonioli, F.; Ferranti, L.; Stocchi, P.; Deiana, G.; Presti, V.L.; Furlani, S.; Marino, C.; Orru, P.; Scicchitano, G.; Trainito, E.; et al. Morphometry and elevation of the last interglacial tidal notches in tectonically stable coasts of the Mediterranean Sea. *Earth-Sci. Rev.* **2018**, *185*, 600–623. [CrossRef]
8. Ferranti, L.; Antonioli, F.; Mauz, B.; Amorosi, A.; Pra, G.D.; Mastronuzzi, G.; Monaco, C.; Orrù, P.; Pappalardo, M.; Radtke, U.; et al. Markers of the last interglacial sea-level high stand along the coast of Italy: Tectonic implications. *Quat. Int.* **2006**, *145–146*, 30–54. [CrossRef]
9. Berger, A.; Loutre, M.-F. Modeling the climate response to astronomical and CO2 forcings. *Comptes Rendus L'acad. Des. Sci.* **1996**, *323*, 1–16.
10. Loutre, M.-F.; Berger, A. Future climatic changes: Are we entering an exceptionally long interglacial? *Clim. Chang.* **2000**, *46*, 61–90. [CrossRef]
11. Berger, A.L. Long-term variations of daily insolation and Quaternary climatic change. *J. Atmos. Sci.* **1978**, *35*, 2362–2367. [CrossRef]
12. Shackleton, N.J.; Hall, M.A.; Vincent, E. Phase relationships between millennial-scale events 64,000–24,000 years ago. *Paleoceanography* **2000**, *15*, 565–569. [CrossRef]
13. Rovere, A.; Raymo, M.E.; Vacchi, M.; Lorscheid, T.; Stocchi, P.; Gómez-Pujol, L.; Harris, D.L.; Casella, E.; O'Leary, M.J.; Hearty, P.J. The analysis of Last Interglacial (MIS 5e) relative sea-level indicators: Reconstructing sea-level in a warmer world. *Earth Sci. Rev.* **2016**, *159*, 404–427. [CrossRef]
14. Berger, A. Climate: An exceptionally long interglacial ahead? *Science* **2002**, *297*, 1287–1288. [CrossRef] [PubMed]
15. Antonioli, F.; De Falco, G.; Lo Presti, V.; Moretti, L.; Scardino, G.; Anzidei, M.; Bonaldo, D.; Carniel, S.; Leoni, G.; Furlani, S.; et al. Relative sea-level rise and potential submersion risk for 2100 on 16 Coastal Plains of the Mediterranean Sea. *Water* **2020**, *12*, 2173. [CrossRef]
16. Ferranti, L.; Antonioli, F.; Monaco, C.; Scicchitano, G.; Spampinato, C.R. Uplifted Late Holocene shorelines along the coasts of the Calabrian Arc: Geodynamic and seismotectonic implications. *Ital. J. Geosci.* **2017**, *136*, 454–470. [CrossRef]
17. Aral, M.M.; Chang, B. Spatial variation of sea level rise at Atlantic and Mediterranean coastline of Europe. *Water* **2017**, *9*, 522. [CrossRef]
18. Fox-Kemper, B.; Hewitt, H.T.; Xiao, C.; Aðalgeirsdóttir, G.; Drijfhout, S.S.; Edwards, T.L.; Golledge, N.R.; Hemer, M.; Kopp, R.E.; Krinner, G.; et al. Ocean, cryosphere and sea level change. In *Climate Change 2021: The Physical Science Basis. Contribution of Working Group I to the Sixth Assessment Report of the Intergovernmental Panel on Climate Change*; Masson Delmotte, V., Zhai, P., Pirani, A., Connors, S.L., Péan, C., Berger, S., Caud, N., Chen, Y., Goldfarb, L., Gomis, M.I., Huang, M., et al., Eds.; Cambridge University Press: Cambridge, UK, 2021.
19. Ferranti, L.; Antonioli, F.; Anzidei, M.; Monaco, C.; Stocchi, P. The timescale and spatial extent of recent vertical tectonic motions in Italy: Insights from relative sea-level changes studies. *J. Virtual Explor.* **2010**, *36*, 23. [CrossRef]
20. Antonioli, F.; Silenzi, S.; Vittori, E.; Villani, C. Sea level changes and tectonic mobility: Precise measurements in three coastlines of Italy considered stable during the last 125 kyrs. *Phys. Chem. Earth* **1999**, *24*, 337–342. [CrossRef]
21. Issel, A. Lembi fossiliferi quaternari e recenti osservati nella Sardegna meriodionale dal Prof. D. Lovisato. *Rend. Accad. Sci.* **1914**, *5*, 759–770.
22. Ulzega, A.; Ozer, A. *Comptes-Rendus de 1'Excursion Table Ronde sur le Tyrsrhénien de Sardaigne*; INQUA. Sous Commission Mediterranee-mer Noire: Cagliari, Italy, 1980; pp. 24–46.
23. Ulzega, A.; Hearty, J.P. Geomorphology, stratigraphy and geochronology of late quaternary marine deposits in Sardinia. *Z. Geomorphol. Suppl.* **1986**, *62*, 119–129.
24. Cobby, D.M.; Mason, D.C.; Davenport, I.J. Image processing of airborne scanning laser altimetry data for improved river flood modelling. *ISPRS J. Photogramm. Remote Sens.* **2001**, *56*, 121–138. [CrossRef]
25. EMODnet. Bathymetry Viewing and Download Service. Available online: https://portal.emodnet-bathymetry.eu/ (accessed on 16 December 2020).
26. Global Mapper—All-in-One GIS Software. Available online: https://www.bluemarblegeo.com/products/global-mapper.php (accessed on 15 April 2020).
27. Lodolo, E.; Galassi, G.; Spada, G.; Zecchin, M.; Civile, D.; Bressoux, M. Post-LGM coastline evolution of the NW Sicilian Channel: Comparing high-resolution geophysical data with Glacial Isostatic Adjustment modeling. *PLoS ONE* **2020**, *15*, e0228087. [CrossRef]
28. Segre, A.G. Linee di riva sommerse e morfologia della piattaforma continentale relativa alla trasgressione marina versiliana. *Quaternaria* **1968**, *11*, 1–14.
29. Orrù, P.E.; Antonioli, F.; Lambeck, K.; Verrubbi, V. Holocene sea-level change in the Cagliari coastal plain (South Sardinia, Italy). *Quat. Nova* **2004**, *8*, 193–210.
30. Peirano, A.; Morri, C.; Bianchi, C.; Aguirre, J.; Antonioli, F.; Calzetta, G.; Carobene, L.; Mastronuzzi, G.; Orrù, P. The Mediterranean coral Cladocora caespitosa: A proxy for past climate fluctuations? *Glob. Planet. Chang.* **2003**, *40*, 195–200. [CrossRef]
31. Deiana, G.; Meleddu, A.; Paliaga, E.; Todde, S.; Orrù, P. Continental slope geomorphology: Landslides and pockforms of Southern Sardinian margin (Italy). *Geogr. Fis. Dinam. Quat.* **2016**, *39*, 129–136. [CrossRef]

32. Antonioli, F.; Anzidei, M.; Lambeck, K.; Auriemma, R.; Gaddi, D.; Furlani, S.; Orrù, P.E.; Solinas, E.; Gaspari, A.; Karinja, S.; et al. Sea-level change during the Holocene in Sardinia and in the northeastern Adriatic (central Mediterranean Sea) from archaeological and geomorphological data. *Quat. Sci. Rev.* **2007**, *26*, 2463–2486. [CrossRef]
33. Buosi, C.; Del Rio, M.; Orrù, P.; Pittau, P.; Scanu, G.G.; Solinas, E. Sea level changes and past vegetation in the Punic period (5th–4th century BC): Archaeological, geomorphological and palaeobotanical indicators (South Sardinia—West Mediterranean Sea). *Quat. Int.* **2017**, *439*, 141–157. [CrossRef]
34. Lecca, L.; Carboni, S. The tyrrhenian section of San Giovanni di Sinis (Sardinia): Stratigraphic record of an irregular single high stand. *Riv. Ital. Paléontol. Strat.* **2007**, *113*. [CrossRef]
35. Orrù, P.E.; Antonioli, F.; Hearty, P.J.; Radtke, U. Chronostratigraphic confirmation of MIS 5 age of a baymouth bar at Is Arenas (Cagliari, Italy). *Quat. Int.* **2010**, *232*, 169–178. [CrossRef]
36. Carboni, S.; Lecca, L.; Hillaire-Marcel, C.; Ghaleb, B. MIS 5e at San Giovanni di Sinis (Sardinia, Italy): Stratigraphy, U/Th dating and "eustatic" inferences. *Quat. Int.* **2014**, *328–329*, 21–30. [CrossRef]
37. Segre, A.G. Il Quaternario del Golfo di Terranova Pausania (Olbia) e la sua fauna malacologica. *Boll. Serv. Geol. Ital.* **1954**, *76*, 45–73.
38. Porqueddu, A.; Antonioli, F.; Rubens, D.; Gavini, V.; Trainito, E.; Verrubbi, V. Relative sea level change in Olbia Gulf (Sardinia, Italy), a historically important Mediterranean harbour. *Quat. Int.* **2011**, *232*, 21–30. [CrossRef]
39. Blanc, A.C. Stratigrafia del Canale Mussolini nell'Agro Pontino. *Soc. Toscana Sci. Nat.* **1935**, *54*, 52–56.
40. Arnoldus-Huyzendveld, A.; Perotto, C.; Sarandrea, P. *I Suoli della Provincia di Latina. Carta, Database e Applicazioni*; Gangemi Editore: Rome, Italy, 2009.
41. Liboni, A. Affioramento fossile con malacofauna tra il Quadrato e Casale Nuovo. Borgo Sabotino—Latina). *Studi Per L'ecologia Del Quat.* **1983**, *25*, 131–134.
42. Hearty, P.J. An inventory of Last Interglacial (sensu lato) age deposits from the Mediterranean Basin: A study of Isoleucine epimerization and U-series dating. *Z. Fur Geomorphol. Suppl.* **1986**, *62*, 51–69.
43. Blanc, A.C.; De Vries, M.; Follieri, M. A first C14 date for the Würm I chronology on the Italian coast. *Quaternaria* **1957**, *4*, 83–89.
44. Dai-Pra, G.; Arnoldus-Huyzendveld, A. Lineamenti stratigrafici, morfologici e podologici della fascia costiera dal fiume Tevere al fiume Astura (Lazio, Italia Centrale). *Geol. Romana* **1984**, *23*, 1–12.
45. Nisi, M.F.; Antonioli, F.; Pra, G.D.; Leoni, G.; Silenzi, S. Coastal deformation between the Versilia and the Garigliano plains (Italy) since the last interglacial stage. *J. Quat. Sci.* **2003**, *18*, 709–721. [CrossRef]
46. Barbieri, M.; Carrara, C.; Castorina, F.; Dai-Pra, G.; Esu, D.; Gliozzi, E.; Paganin, G.; Sadori, L. Multidisciplinary study of Middle–Upper Pleistocene deposits in a core from the Piana Pontina (central Italy). *G. Geol.* **1999**, *61*, 47–73.
47. Antonioli, F.; Dai-Pra, G.; Hearty, P.J. I sedimenti quaternari nella fascia costiera della Piana di Fondi (Lazio meridionale). *Boll. Soc. Geol. Ital.* **1988**, *107*, 491–501.
48. Blanc, A.C.; Segre, A.G. Le Quaternaire du Mont Circe'. Livret Guide "Excursion au Mont Circe". In Proceedings of the IV International Meeting INQUA, Rome, Italy, 16–20 September 1953; pp. 23–108.
49. Segre, A.G. Nota sui rilevamenti eseguiti nel Foglio 158 Latina della Carta Geologica d'Italia. *Boll. Serv. Geol. It.* **1957**, *73*, 569–584.
50. Durante, S. Sul Tirreniano e la malacofauna della Grotta del Fossellone (Circeo). *Quaternaria* **1975**, *18*, 331–347.
51. Hearty, P.J.; Dai-Pra, G. Aminostratigraphy of Quaternary marine deposits in the Lazio region of central Italy in Dating Mediterranean shoreline. *Z. Für Geomorphologie. Suppl.* **1986**, *62*, 131–140.
52. Bigi, G.; Casentino, D.; Parlotto, M. *Modello Litostratigrafico-Strutturale della Regione Lazio. Scala 1:250.000*; Geological Map of Regione Lazio, Università degli Studi di Roma "La Sapienza": Rome, Italy, 1988.
53. Serva, L.; Brunamonte, F. Subsidence in the Pontina Plain, Italy. *Bull. Int. Assoc. Eng. Geol.* **2006**, *66*, 125–134. [CrossRef]
54. Blanc, A.C. Una spiaggia pleistocenica a Strombus bubonius presso Palidoro (Roma). *Rend. Accad. Naz. Lincei* **1936**, *23*, 200–204.
55. Farina, S. Late Pleistocene-Holocene mammals from "Canale delle Acque Alte (Canale Mussolini)" (Agro Pontino, Latium) B. *Soc. Paleontol. Ital.* **2011**, *50*, 11–22.
56. Antonioli, F.; Presti, V.L.; Rovere, A.; Ferranti, L.; Anzidei, M.; Furlani, S.; Mastronuzzi, G.; Orru, P.E.; Scicchitano, G.; Sannino, G.; et al. Tidal notches in Mediterranean Sea: A comprehensive analysis. *Quat. Sci. Rev.* **2015**, *119*, 66–84. [CrossRef]
57. Hearty, P.J.; Rovere, A.; Sandstrom, M.R.; O'Leary, M.J.; Roberts, D.; Raymo, M.E. Pliocene-pleistocene stratigraphy and sea-level estimates, republic of South Africa with implications for a 400 ppmv CO 2 World. *Paleoceanogr. Paleoclimatol.* **2020**, *35*, 7. [CrossRef]
58. Gilford, D.M.; Ashe, E.; DeConto, R.M.; Kopp, R.E.; Pollard, D.; Rovere, A. Could the last interglacial constrain projections of future antarctic ice mass loss and sea-level rise? *J. Geophys. Res. Earth Surf.* **2020**, *125*. [CrossRef]
59. Ashkenazy, Y.; Eisenman, I.; Gildor, H.; Tziperman, E. The effect of Milankovitch variations in insolation on equatorial seasonality. *J. Clim.* **2010**, *23*, 6133–6142. [CrossRef]
60. Kirkby, J. Cosmic Rays and Climate, Surveys in Geophysics. Available online: http://arxiv.org/PS_cache/arxiv/pdf/0804/0804.1938v1.pdf (accessed on 26 March 2008).
61. Manara, V.; Brunetti, M.; Celozzi, A.; Maugeri, M.; Sanchez-Lorenzo, A.; Wild, M. Detection of dimming/brightening in Italy from homogenized all-sky and clear-sky surface solar radiation records and underlying causes (1959–2013). *Atmos. Chem. Phys. Discuss.* **2016**, *16*, 11145–11161. [CrossRef]

62. Marsh, G.E. Interglacials, Milankovitch cycles, solar activity, and carbon dioxide. *J. Clim.* **2014**, *2014*, 345482. [CrossRef]
63. Smulsky, J.J. A new theory of change in the insolation of the earth over millions of years against marine isotope stages. *Izv. Atmos. Ocean. Phys.* **2020**, *56*, 721–747. [CrossRef]